Dalton Transactions

ROYAL SOCIETY OF CHEMISTRY

PAPER

View Article Online
View Journal | View Issue

Cite this: *Dalton Trans.*, 2022, **51**, 4135

Use of group 13 aryloxides for the synthesis of green chemicals and oxide materials†

Rafał Petrus,*[a] Józef Utko,[b] Joanna Petrus,[c] Mohammad Awashra[d] and Tadeusz Lis[b]

Received 8th November 2021,
Accepted 8th February 2022

DOI: 10.1039/d1dt03777c

rsc.li/dalton

In this work, group 13 metal aryloxides [Al(MesalO)$_3$] (**1**), [Me$_2$Ga(MesalO)]$_2$ (**2**), [AlLi$_3$(MesalO)$_6$] (**3**) and [Me$_2$GaLi(MesalO)$_2$(THF)] (**4**) were obtained by the reaction of methyl salicylate (MesalOH) with group-13 alkyls MMe$_3$ (for M = Al, Ga) or their combination with BuLi in a THF/alcohol solution. The direct reaction of MMe$_3$ (for M = Al, Ga) and MesalOH (1 : 3) led to compound **1** or **2**, respectively. When the same reactions were carried out with additional BuLi, the heterometallic compound **3** or the mixture of **4** and [Li$_6$(MesalO)$_6$] (**5**) was obtained. Compounds **1–5** were used for the chemical conversion of glycerol to α-hydroxy acid glyceryl esters by alcoholysis of L-lactide (L-LA), glycolide (GA), and ε-caprolactone (ε-CL). Compounds **1–5** were also efficient initiators for the ring-opening polymerization (ROP) of L-LA, GA, and ε-CL using glycerol as a branching agent to synthesize 3-arm polyesters. Heterometallic compounds **3** and **4** were attractive molecular precursors for the preparation of group 13-lithium ceramics, *i.e.* γ-LiAlO$_2$ and β-LiGaO$_2$.

Introduction

Glycerol is an important raw material with extensive applications in the petrochemical, tobacco, food, cosmetic and pharmaceutical industries, *i.e.*, as a food preservative and filler, sweetener, thickener, solvent, humectant, lubricant, demulcent, emollient, and antimicrobial and antiviral agents. It is also a major by-product of the conversion of vegetable oils to biodiesel. In the last ten years, increased biodiesel production has led to a glut of glycerol in the global market.[1] Therefore, many routes or technologies have been implemented to transform crude glycerol into value-added chemicals or to use it for viable energy generation. The most common reactions are hydrogenolysis, esterification, etherification, selective oxidation or reduction, dehydration, pyrolysis, and gasification.[2–4] Glycerol is usually converted into glyceryl esters, glyceric acid, 1,2-propanediol, dihydroxyacetone, mesoxalic acid, oxalic acid, tartronic acid, glycerol carbonate,[5] polyglycerols, syngas, or hydrogen.[6,7] Macromolecular glycerol derivatives are attracting increased attention due to the diversity of polymer compositions and architectures. Linear, hyperbranched, or dendritic glycerol-based polyethers, polycarbonates, and polyhydroxyacids were investigated mainly for the delivery of therapeutic agents. For example, poly(glycerol sebacate) was essential for cardiovascular, neurovascular, orthopedic, and soft tissue regeneration systems.[8] Glycerol or polyglycerols were also applied as branching agents to synthesize aliphatic biodegradable polyesters for encapsulation purposes.[9–12] Star-shaped glycerol-lactic acid oligomers were used for the surface modification of hygienic superabsorbent polymer hydrogels.[13] Low molecular weight lactic acid glyceryl derivatives were investigated as dietary energy supplements,[14] active ingredients in antiseptic and antimicrobial compositions,[15] or promising plasticizers for poly(L-lactide) (PLLA). Plasticized PLLA had a lower glass transition temperature, 3.8 times greater elongation at break, and 1.7 times greater impact strength.[16] Glyceryl glycolates were developed as anti-aging skin care ingredients in cosmetics. Glyceryl esters have high valorization potential and remarkable properties and can be applied as additives or precursors in many processes in the polymer field. Therefore, great interest has been focused on developing novel and inexpensive synthesis methods or new areas of their practical application.

Based on the above, we chose glycerol as the external alcohol and branching agent to synthesize α-hydroxy acid glyceryl esters or star-shaped polyesters. We decided to explore the use of group 13 metal aryloxides because they are popular catalysts/initiators in organic synthesis[17–20] and polymeriz-

[a]*Faculty of Chemistry, Wrocław University of Science and Technology, 23 Smoluchowskiego, 50-370 Wrocław, Poland. E-mail: rafal.petrus@pwr.edu.pl*
[b]*Faculty of Chemistry, University of Wrocław, 14 F. Joliot-Curie, 50-383 Wrocław, Poland*
[c]*Maco Productions Polonia, 22 Szwajcarska, 54-405 Wrocław, Poland*
[d]*Department of Chemistry, Aix-Marseille University, Jardin du Pharo, 58 bd Charles Livon, 13284 Marseille Cedex 07, France*

†Electronic supplementary information (ESI) available. CCDC 2076392–2076396, 2128614 and 2128703. For ESI and crystallographic data in CIF or other electronic format see DOI: 10.1039/d1dt03777c

ation reactions.[21–33] Recently, our interest has been focused on the synthesis of heterometallic compounds, in which the presence of two different Lewis centers can result in heterometallic cooperativity.[34–38] For example, chiral lithium–aluminum binaphthoxide [AlLi(binol)$_2$] is a highly effective asymmetric catalyst for the 1,4-addition of a Horner–Wadsworth–Emmons reagent to enones, Michael additions, and tandem Michael-aldol reactions.[39,40] The heterobimetallic gallium–lithium catalyst [GaLi((binol-CH_2)$_2$O)] was used for the enantioselective *meso*-epoxide ring-opening reaction with a phenolic oxygen nucleophile to afford 1,2-diol monoethers in up to 94% yield and up to 96% *ee*.[41] Although group 13-lithium aryloxides/alkoxides have been well studied in a range of organic transformations, the examples of heterometallic cooperativity in polymerization processes are limited. Within the selected group of compounds, only six aluminum and two indium derivatives have been investigated for the ROP of cyclic esters.[42] Among them, sterically hindered anionic aluminum–lithium alkoxide complexes supported by diamido ether tridentate ligands [HAlLi(OBn)((RN-*o*-C_6H_4)$_2$O)(THF)$_2$] (R = C_4H_9, Cy) were inactive in the ROP of *rac*-LA; however, their bis-alkoxide analogs [AlLi(OBn)$_2$((RN-*o*-C_6H_4)$_2$O)(THF)$_2$] polymerized 85% of the monomer in 16 h (*rac*-LA/Al = 230/1, 25 °C, CH_2Cl_2).[43] For heterometallic aluminum aryloxides [Me_2AlM(2,6-(MeO)$_2C_6H_3O$)$_2$]$_2$ (M = Li, Na, K), a higher activity in the ROP of L-LA (L-LA/Al/BnOH = 100/1/1, 5 h, 125 °C, toluene) of the lithium analogue (78%) than those of sodium (48%) and potassium (20%) was observed.[44] Lithium–indium complexes supported by dianionic fluorinated dialkoxy-diimino ligands {ONRNO}$^{2-}$ (R = C_2H_4, *rac*-1,2-cyclohexyl) converted 98–99% of *rac*-LA in 16 or 0.5 h (*rac*-LA/In/iPrOH = 100/1/1, 80 °C, toluene) but polymerization control was poor in both cases.[45] The essential common feature of these compounds is that they are more active than their homometallic trivalent counterparts. Recently, the Williams group reported a series of heterodinuclear Al(III)/M(I) Schiff base catalysts (M = Na, K, Rb, Cs), which show exceptional activities for phthalic anhydride and cyclohexene oxide copolymerization. The best synergic heterometallic cooperation shows the Al(III)/K(I) catalyst (TOF = 1072 h^{-1}, 0.25 mol% *vs.* anhydride, T = 100 °C) that combines high activity, quantitative alternating polyester selectivity, and excellent polymerization control at catalyst loadings below 1 mol%.[46] Therefore, the development of new group 13-lithium complexes and their applications in the polymerization of cyclic esters are essential to understand the important catalyst features in heterometallic cooperativity.

Heterometallic group 13-lithium alkoxides are also attractive single-source molecular precursors to prepare $LiMO_2$ (for M = Al, Ga) ceramics by a hydrothermal or sol–gel process.[47,48] Among the materials of this group, special attention has been focused on γ-$LiAlO_2$ and β-$LiGaO_2$, which have unique physicochemical properties and a wide range of practical applications. γ-$LiAlO_2$ is an essential material in battery technologies and is used to coat electrodes[49,50] or used as an electrolyte matrix in molten carbonate fuel cells.[51] Due to its chemical and thermal stability and good performance under high neutron and electron radiation, it is also considered a promising tritium breeder in nuclear fusion reactors.[52] β-$LiGaO_2$ doped with V^{3+} or Cr^{4+} ions is an attractive tunable room-temperature laser material. β-$LiGaO_2$-ZnO alloys form semiconductors with a tunable direct bandgap between 3.3 and 5.6 eV and therefore were applied to fabricate laser diodes and photodetectors operating throughout much of the ultraviolet region.[53,54] β-$LiGaO_2$ and γ-$LiAlO_2$ were also investigated as lattice-matched substrates for epitaxial growth of GaN,[55,56] InN,[57] and ZnO.[58,59]

Here, we report a new method of chemical conversion of glycerol to α-hydroxy acid glyceryl esters by alcoholysis of cyclic esters, *i.e.*, L-lactide (L-LA), glycolide (GA), and ε-caprolactone (ε-CL), mediated by lithium and group 13 aryloxides. The preparation and characterization of six metal aryloxides, namely [Al(MesalO)$_3$] (**1**), [Me_2Ga(MesalO)]$_2$ (**2**), [$AlLi_3$(MesalO)$_6$] (**3**), [Me_2GaLi(MesalO)$_2$(THF)] (**4**), [Li_6(MesalO)$_6$] (**5**) and [Me_2GaLi(MesalO)$_2$(H_2O)] (**6**), MesalO = methyl salicylate ligand, are presented. Compounds **1–5** are effective initiators for the ROP of L-LA, GA, and ε-CL using glycerol as a branching agent to synthesize 3-arm polyesters. Compounds **3** and **4** were found to be attractive molecular precursors for the preparation of group 13-lithium ceramics, *i.e.* γ-$LiAlO_2$ and β-$LiGaO_2$.

Results and discussion

Synthesis and characterization of homometallic and heterometallic group 13 metal aryloxides

We focused on designing homo- and heterometallic compounds with a well-defined molecular structure obtained by the reaction of organometallic reagents of group 13 or lithium with a phenolic ligand. The selection of suitable ligands that would positively influence the solubilities and crystallization abilities of metal compounds was essential. We investigated methyl salicylate as a potential ligand because, after deprotonation, it can act as an O,O′-bidentate chelating agent for a number of metal ions, forming thermodynamically stable and neutral complexes.[60–63] We also chose methyl salicylate for its commercial availability, low cost, and properties that allow its use in many industrial applications, including medicine, food, and cosmetics.[64,65]

Our interest in synthesizing group 13 metal aryloxides arose from a simple reaction between $AlMe_3$ and MesalOH (1 : 3) performed in a THF/MeOH solution (1 : 2). After several weeks of crystallization, colorless plate crystals of [Al(MesalO)$_3$] (**1**, 65%) were obtained. Previously, Lewiński reported the synthesis of aluminum methyl salicylate compounds of [Me_2Al(MesalO)]$_2$ and [MeAl(MesalO)$_2$] by the selective substitution of one or two Me groups in $AlMe_3$ using the MesalOH proligand.[66,67] We found that the introduction of MeOH into the synthesis procedure leads to the substitution of all alkyl groups in $AlMe_3$. We then decided to use $GaMe_3$ for comparison with $AlMe_3$, but dimeric dimethyl-gallium aryloxide [Me_2Ga(MesalO)]$_2$ (**2**, 69%) was obtained as shown in Scheme 1.

It is well-established that the direct reaction of trialkylgallium reagents with phenols usually leads to the formation of

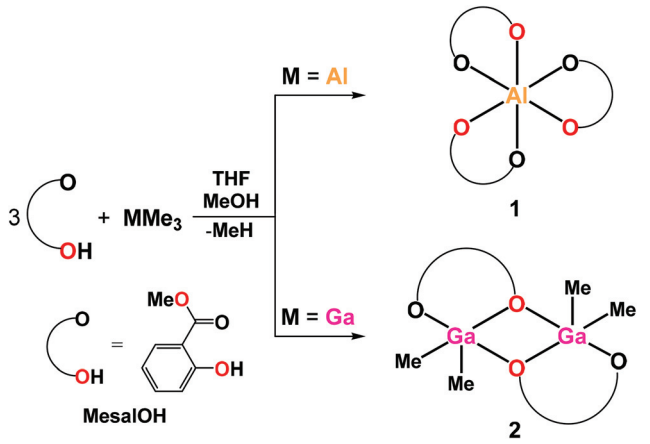

Scheme 1 Synthesis of **1** and **2**.

dialkylgallium(aryloxides) $[Me_2Ga(OAr)]_2$. The lack of further reaction is probably due to electronic effects because the strong electron-donating aryloxide in $[Me_2Ga(OAr)]_2$ reduces the reactivity of Ga–Me bond towards protonolysis. When an elevated temperature (above 100 °C) was used, the synthesis of alkylgalliumbis(aryloxides) $[MeGa(OAr)_2]$, OAr = halido substituted 8-quinolinato, was also reported.[68] There are no known examples of gallium trisaryloxide synthesized using organometallic reagents.[69,70] In this work, all reactions involving the use of $GaMe_3$ were carried out at room temperature, and the substitution of only one methyl group was observed.

Single-crystal X-ray diffraction (XRD), NMR spectroscopy, and Fourier-transform infrared attenuated total reflectance (FTIR-ATR) spectroscopy were used to determine the structures and physicochemical properties of the compounds obtained [ESI, Table S1 and Fig. S1–S6†]. The molecular structure of **1** presented in Fig. 1 revealed a distorted octahedral geometry around Al1 atoms with the O_6 donor surrounding three MesalO ligands. It should also be noted that in coordination chemistry AlO_6 octahedra are observed only in three mononuclear aluminum aryloxides $[Al(OAr)_3]$ for OAr = 1-(4-methoxy-2-oxyphenyl)ethanonato;[71] 3,6-di-*t*-butyl-1,8-diazatricyclo[6.2.2.0^{2,7}]dodeca-2,4,6-triene-4,5-diolato; 9-oxy-1*H*-phenalen-1-one;[72] and 2-oxybenzaldehydato.[73] The lengths of the Al–$O_{(aryloxo)}$ bonds, *i.e.*, 1.817(3)–1.824(4) Å, are typical of octahedrally coordinated aluminum centers.[74–76] The results of continuous-shape measure calculations showed an insignificant departure from an ideal octahedron for the coordination environment around Al1 with the *S*(Oh) parameter of 0.170.[77]

The mononuclear coordination aluminum compound $[Al(EtsalO)_3]$ (**1a**, 56%) (where EtsalO = ethyl salicylate ligand), was also synthesized using EtOH instead of MeOH (ESI, Table S1 and Fig. S7–S10†).

The structure of **2** was previously published together with the aluminum and indium isostructural analogs.[67] However, the data deposited in the Cambridge Structural Database were obtained at room temperature, unlike the structure of **2** determined by us at 100 K. Therefore, we introduced a detailed

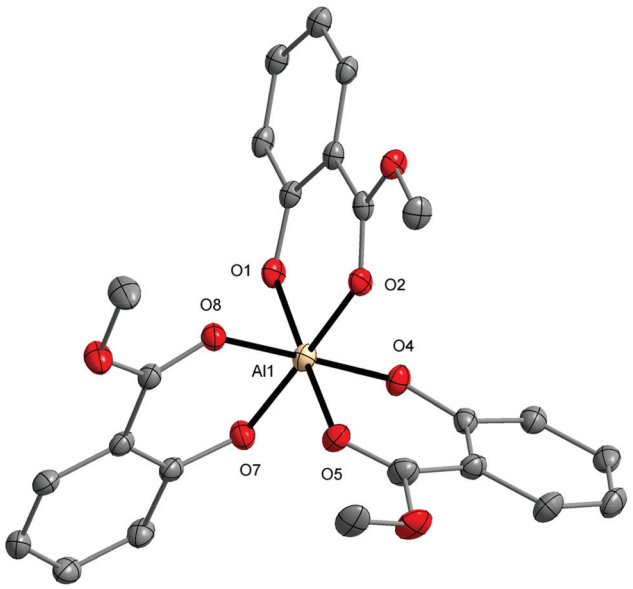

Fig. 1 Molecular structure of $[Al(MesalO)_3]$ (**1**). Displacement ellipsoids are drawn at the 25% probability level. The second part of the disordered aryloxy ligands and hydrogen atoms are omitted for the sake of clarity.

description of the received molecular model in this work (Fig. 2). The lengths of Ga–$O_{(aryloxo)}$, *i.e.*, 1.936(2)–2.275(2) Å and Ga-CH_3 of 1.956(2)–1.958(2) Å are typical of alkoxo/aryloxo bridged dimeric gallium compounds.[78–81] The comparison of Ga–O distance in the equatorial plane (1.936(2) Å) with those in the axial plane (2.161(2) and 2.275(2) Å) revealed the significant lengthening of axial Ga–O bonds, which results from the low Lewis acidity of the gallium(III) ions. The gallium atoms in **2** adopt a distorted trigonal bipyramidal geometry with *S*(TBPY-5) = 1.262. Dialkyl(aryloxides) of group 13 have been intensively investigated in the past as reagents in metal–organic chemical vapor deposition and various inorganic/organic transformations.[82–86]

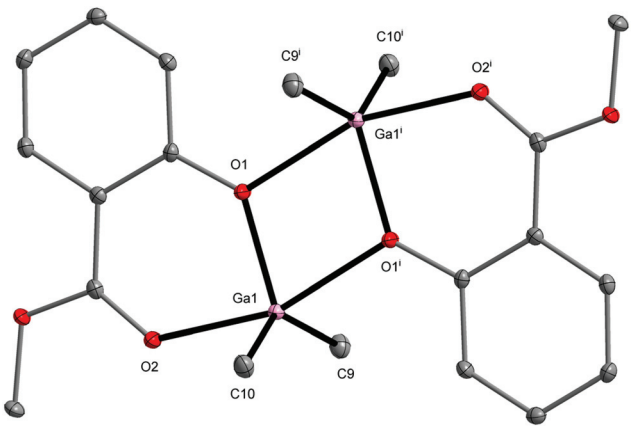

Fig. 2 Molecular structure of $[Me_2Ga(MesalO)]_2$ (**2**). The displacement ellipsoids are drawn at the 30% probability level. Hydrogen atoms are omitted for the sake of clarity [symmetry code: (i) $-x + 1, -y + 1, -z + 1$].

We investigate the synthesis of group 13-lithium aryloxides by the reaction of the ligand precursor with MMe_3 (for M = Al, Ga) and BuLi, in a solution of THF/MeOH at stoichiometries of M/Li/MesalOH = 1/3/6, as shown in Scheme 2.

The XRD study of the received crystalline materials showed the formation of $[AlLi_3(MesalO)_6]$ (**3**, 54%) or the mixture of $[Me_2GaLi(MesalO)_2(THF)]$ (**4**, 25%) and $[Li_6(MesalO)_6]$ (**5**, 64%). Compounds **3** and **4** were characterized by ^1H, ^{13}C, ^1H-DOSY, and ^7Li NMR, and FTIR-ATR spectroscopy (ESI, Fig. S11–S20†).

Aluminum and lithium ions in **3** held together by four μ- and two μ_3-$O_{(aryloxo)}$ bridges form a double-opened dicubane core structure with two missing vertices. In this structure, the Li1–Li3 ions occupy two external vertices and one vertex of the common face of the tetranuclear unit. The second vertex of the common face is the Al1 ion (Fig. 3).

In coordination chemistry, heterometallic aluminum–lithium aryloxides usually form dinuclear or tetranuclear compounds with an Al : Li ratio of 1 : 1, *i.e.*, $[Me_2AlLi(OAr)_2]$,[87] and $[MeAlLi(OAr)(OCMePhPh)(Et_2O)]$[88] where OAr = 2,6-di-*t*-butyl-4-methylphenoxide; $[AlLi(EDBP)_2(THF)_2]$ where EDBP = 2,2′-ethylidenebis(4,6-di-*tert*-butylphenolato);[89] $[AlLi(binol)(THF)_2((CH_2)_5CO)]$;[39] $[AlLi(binol)(O^tBu)_2(PMDTA)]$ where PMDTA = *N*,*N*′,*N*″,*N*″-pentamethyldiethylenetriamine, $[AlLi(binol)(O^tBu)_2(THF)_2]$, $[Al_2Li_2(binol)_4(THF)_4]$;[90] $[Me_2AlLi(OAr)_2]_2$ where OAr = 2,6-dimethoxyphenoxide,[91] $[Et_2Al_2Li_2(OAr)_4(DME)_3]_n$ where OAr = catecholato.[92] For the Al : Li ratio of 2 : 1 or 1 : 3, only the structures of $[R_2Al_2Li(OPh)_6(THF)_6]$ (for R = Et, ^nBu),[93] or $[AlLi_3(binol)_3(THF)_6]$[90] have been reported. For heterometallic aluminum–lithium compounds, the double open dicubane unit was observed only in the structure of $[Al_2Li_2(OR)_8]$ for RO = hexafluoropropoxide.[94] The Li1 and Li2 atoms in **3** adopt a trigonal

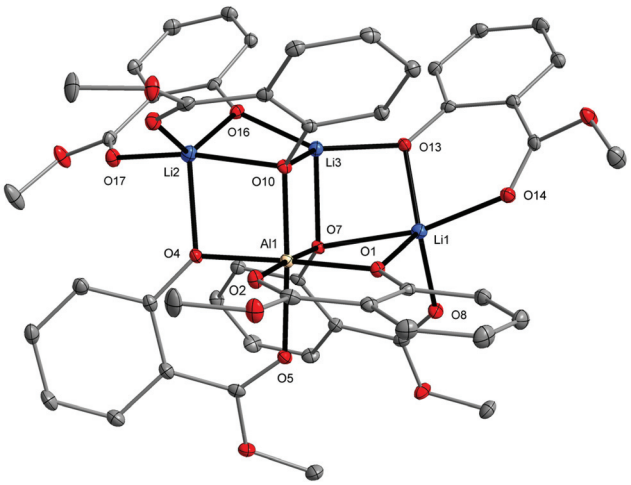

Fig. 3 Molecular structure of $[AlLi_3(MesalO)_6]$ (**3**). The displacement ellipsoids are drawn at the 30% probability level. Hydrogen atoms are omitted for the sake of clarity.

bipyramidal geometry with the metric parameters *S*(TBPY-5) = 2.047 or 1.717, while the Li3 atom forms a vacant trigonal bipyramid (*S*(vTBPY-4) = 4.723). The six-fold coordinated Al1 atom with the O_6 donor environment adopted an octahedral geometry (*S*(Oh) = 0.256). The ^1H and $^{13}C\{^1H\}$ NMR spectra of **3** in THF-D_8 revealed the presence of two sets of nonequivalent resonance signals with the 2 : 1 ratio corresponding to four μ-MesalO and two μ_3-MesalO ligands (ESI, Fig. S11 and S12†). The ^7Li NMR spectrum of **3** contains only one signal at 4.00 ppm (ESI, Fig. S13†). The DOSY ^1H NMR spectra of **3** and **4** revealed the retention of solid-state structures in the THF-D_8 solution (ESI,

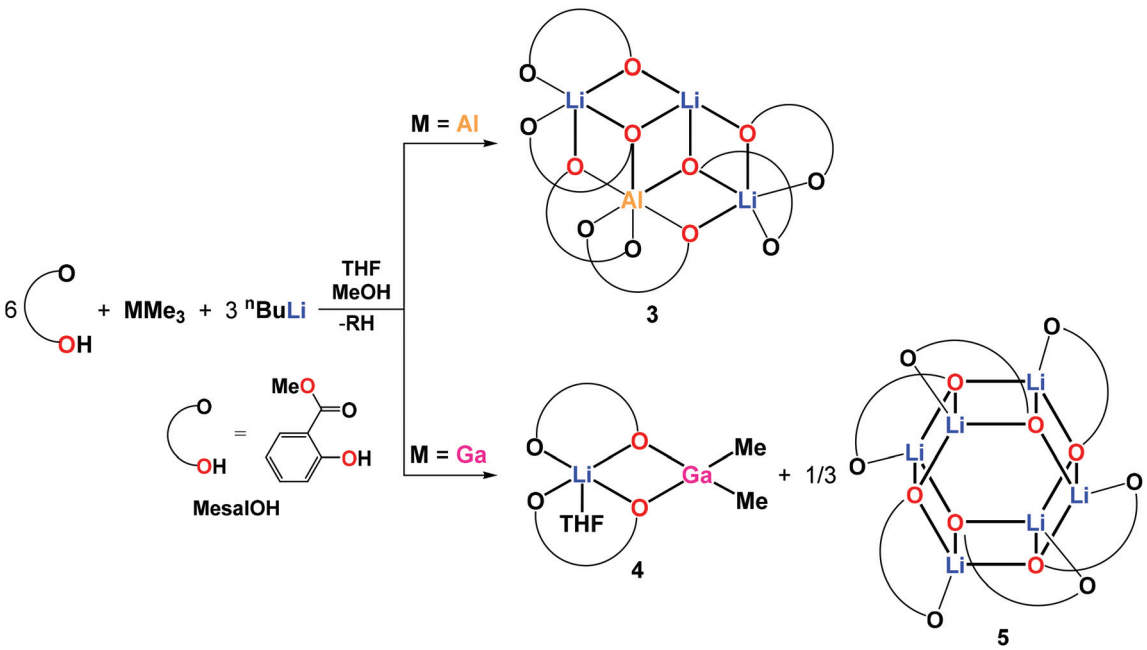

Scheme 2 Synthesis of **3**–**5**.

Fig. S14 and S19†). When for the synthesis of aluminum–lithium compound **3** EtOH was used instead of MeOH, the isostructural compound $[AlLi_3(EtsalO)_6]$ (**3a**, 63%) was obtained (ESI, Table S1, Fig. S21–S25†).

The molecular structure of **4** formally consists of units $\{Me_2Ga(MesalO)\}$ and $\{Li(MesalO)(THF)\}$ bridged by aryloxo oxygen atoms. The metal atoms in **4** adopt a distorted tetrahedral geometry (Ga1 with S(T-4) = 2.116) or a square pyramidal geometry (Li1 with S(SPY-5) = 0.643).[95] The dinuclear gallium–lithium structure has previously been reported for $[GaLi(MTB)_2(THF)_3]$ where MTB = 2-oxo-2′-mercapto-1,1′-binaphthyl,[96] and $[GaLi(OR)_4(THF)_2]$ where RO = 2-trifluoromethyl-2-propanolato.[97] Heterometallic gallium–lithium alkoxides/aryloxides usually form tetranuclear clusters, *i.e.* $[GaLi_3(binol)_3(THF)_4]$, $[GaLi_3(binol)_3(DME)_3]$,[98] or $[Me_2GaLi(OR)_2]_2$ for RO = 2-methoxyethanolato.[99] We also investigated the reactivity of alkyl groups in **4** by performing an NMR-scale reaction in THF-D_8 solution with four molar equiv. of MeOH. These measurements revealed that Ga–Me bonds remain intact, and no evolution of methane was detected (ESI, Fig. S26†). When the crystals of compound **4** were exposed to air overnight, colorless needle-like crystals of $[Me_2GaLi(MesalO)_2(H_2O)]$ (**6**) were obtained (ESI, Fig. S27†). In **6**, the water molecule coordinated to the lithium center replaces the THF molecule observed in **4** (Fig. 4).

The presence of two different metal elements in the structures of **3** and **4** makes them ideal candidates for use as molecular precursors to prepare group 13-lithium ceramics. Thermogravimetry and differential scanning calorimetry (TGA-DSC) were used to select the calcination temperatures required for the efficient removal of organic ligands and crystallization of heterometallic oxide phases. The thermal decompositions of compounds **3** and **4** from 25 to 1000 °C were performed with a heating rate of 10 °C min^{-1} under N_2. The thermograms obtained presented in Fig. 5 indicate that compounds **3** and **4** underwent multistep thermal decomposition. The melting points of **3** and **4** determined by DSC were 200.5 °C and 124.4 °C, respectively. Compound **3** was stable up to 175 °C with a mass loss not exceeding 1%. For **4**, the decomposition starts above 95 °C with the removal of the THF ligand. The aromatic ligands were decomposed and removed within 190 and 300 °C for **4** and 190 and 500 °C for **3**. The overall mass loss of 84.8% for **3** corresponds well to the estimated value of 85.4% for the equimolar mixture of $LiAlO_2$ and Li_2CO_3. The thermal decomposition of **4** with a mass loss of 76.9% compared to the theoretical value of 77.4% indicated the formation of $LiGaO_2$. The final thermal decomposition temperatures were 850 °C for **3** and 751 °C for **4**.

The PXRD patterns (Fig. 6) of oxide materials synthesized by calcination of **3** at 850 °C show the formation of γ-$LiAlO_2$ as the main crystalline phase and small amounts of Li_2CO_3 (Fig. 6a). The resulting raw powder was then purified using the different water solubilities of both phases. The water-soluble Li_2CO_3 was removed by solvent extraction to give pure γ-$LiAlO_2$ as shown in Fig. 6b. Thermolysis of **4** at 850 °C leads to the selective formation of β-$LiGaO_2$ as shown in Fig. 7. The morphology of the resulting heterometallic oxide materials was investigated by transmission electron microscopy (TEM, Fig. 8, 9 and Fig. S28, S29 in the ESI†). The γ-$LiAlO_2$ crystallites of diameter 36–45 nm are oval with a marked tendency for aggregation (Fig. 8). The β-$LiGaO_2$ crystallites with a 35–400 nm size are well-dispersed and oval or spherical (Fig. 9).

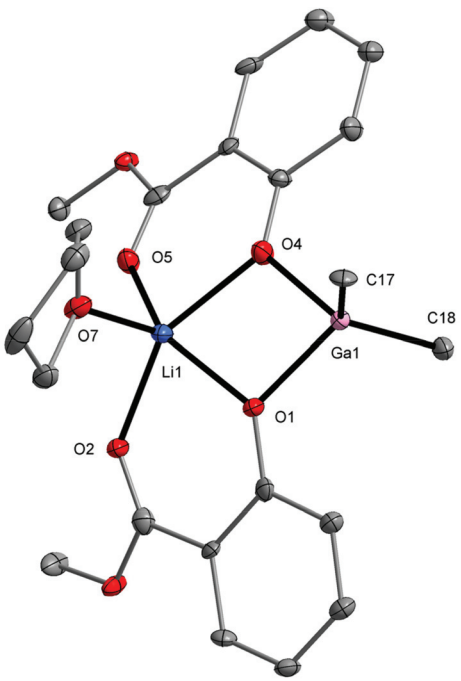

Fig. 4 Molecular structure of $[Me_2GaLi(MesalO)_2(THF)]$ (**4**). The displacement ellipsoids are drawn at the 30% probability level.

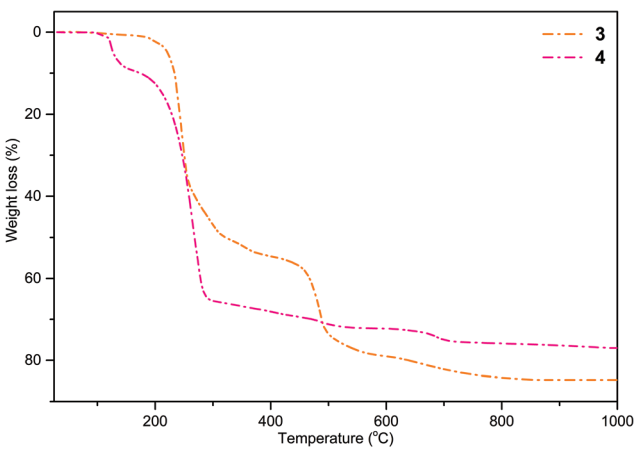

Fig. 5 TGA curves for **3** and **4** measured at a heating rate of 10 °C min^{-1} under a nitrogen atmosphere over the temperature range 25–1000 °C.

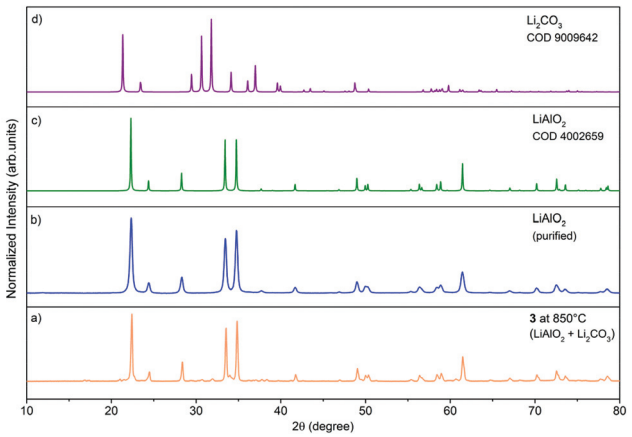

Fig. 6 PXRD patterns of materials prepared by calcination of **3** at 850 °C (a), purified γ-$LiAlO_2$ (b), γ-$LiAlO_2$ [Crystallography Open Database (COD), 4002659, green] (c), Li_2CO_3 [COD, 9009642, purple] (d).

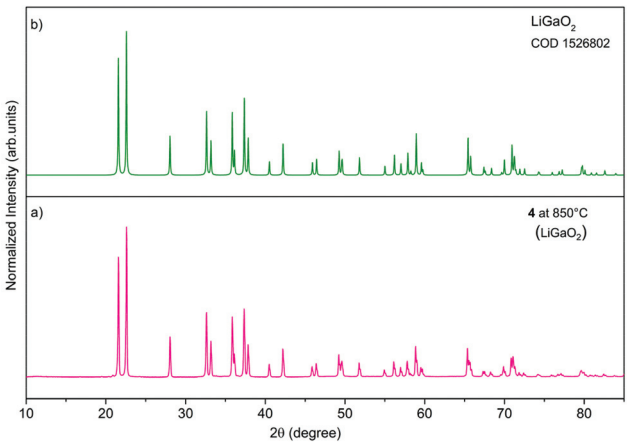

Fig. 7 PXRD patterns of the material prepared by calcination of **4** at 850 °C (a), β-$LiGaO_2$ [COD, 1526802, green] (b).

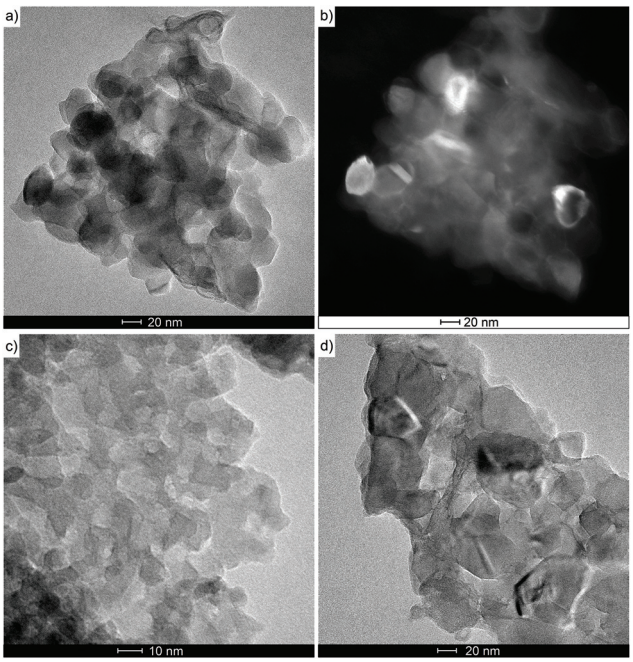

Fig. 8 TEM micrographs of γ-$LiAlO_2$ prepared by calcination of **3** at 850 °C (a–d).

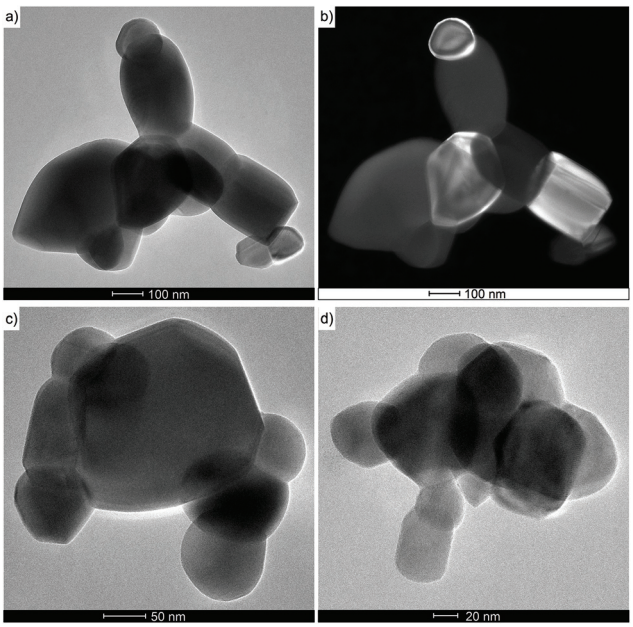

Fig. 9 TEM micrographs of β-$LiGaO_2$ prepared by calcination of **4** at 850 °C (a–d).

Alcoholysis of cyclic esters

We investigated the alcoholysis reactions of heterocyclic esters, namely L-LA, GA, and ε-CL, to synthesize α-hydroxy acid glyceryl esters (Scheme 3). Typical reactions were carried out in a THF solution at room temperature using 1 to 3 equivalents of glycerol (Gl) per lactone and **1–5** as catalysts.

First, we conducted control experiments for the selected heterocyclic esters in the absence of a catalyst source. ^{1}H NMR monitoring of alcoholysis reactions with a stoichiometry of X/Gl = 1/3 for X = L-LA, GA and ε-CL over time showed that after 168 h, 93% conversion of L-LA to glyceryl (*S*,*S*)-*O*-lactyllactate (GlL_2) and 99% conversion of GA to the mixture of glyceryl glycolylglycolate (GlG_2, 55%) and glyceryl tris(glycolyl)glycolate (GlG_4, 44%) were obtained (ESI, Table S2, entry 27 and Table S3 entry 23, Fig. S30–S33†). Under these conditions, no reactivity of ε-CL was observed. When the same reactions were performed using only two molar excess of Gl, a significant decrease in the conversion of heterocyclic esters was observed, 70% for GlL_2 and 40%/43% for GlG_2/GlG_4 (ESI, Table S2 entry 16 and Table S3† entry 15). All reactions were carried out using an excess of Gl, and therefore, monoglyceryl esters of hydroxy acids were predominantly formed. However, the formation of 1-monoglyceryl and 2-monoglyceryl esters of hydroxy acids was

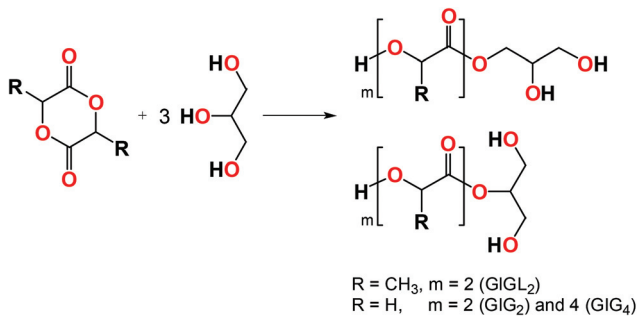

Scheme 3 Catalyst-free alcoholysis of L-LA and GA.

observed in the investigated reactions, as shown in Scheme 3. In this work, both isomers were treated as one kind of product. We cannot rule out the formation of di- and triglyceryl esters of hydroxy acids, but their presence was not observed in the amounts detectable by NMR spectroscopy.

When L-LA alcoholysis reactions were carried out with the stoichiometry of L-LA/Gl/M = 1/3/0.01, where M is a metal atom present in compounds **1–4**, the results obtained were similar to those for catalyst-free reactions (ESI, Table S4,† entries 1–4). Under similar conditions, after 360 min, **5** led to the mixture of glyceryl lactate (GlL_1) and GlL_2 49/47% (ESI, Table S4,† entry 18). The catalyst concentration increased five times; compounds **3** and **4** converted 94–99% of L-LA in 2 minutes. After 30 min, the mixture of GlL_1/GlL_2 with individual conversion yields of 62%/37% for **3** and 8%/90% for **4** was achieved (ESI, Table S4, entries 28–35; Fig. S34 and S35†). Compounds **1** and **2** were inactive in this reaction, and **5** led to lactyl oligomers.

In GA alcoholysis reactions carried out with the GA/Gl/M = 1/3/0.01 stoichiometry using compounds **1–5**, >98% substrate conversion was observed within the first 5 min. In the initial stage of these reactions, metal-aryloxide catalysts led to the formation of glycolic acid oligoesters (GlG_n), which were then converted into glyceryl glycolate (GlG_1) and GlG_2 (ESI, Fig. S36–S38†). For example, after 30 min, the conversion of GA to $GlG_1/GlG_2/GlG_n$ was 4/56/40% for **1**, 85/13/2% for **3**, 64/24/11% for **4**, and 63/26/11% for **5** (ESI, Table S5,† entries 5, 14, 21 and 33).

When the ε-CL alcoholysis reactions were carried out with the ε-CL/Gl/M = 1/2/0.08 stoichiometry after 300 min conversion of ε-CL into glyceryl 6-hydroxyhexanoate ($GlCL_1$) was 60% for **3** and 77% for **4** (ESI, Table S6, entries 28 and 33, Fig. S39–S41†). Compounds **1** and **2** were inactive under the investigated conditions, and **5** in the reaction when using ε-CL/Gl/M = 1/2/0.02 after 96 min converts 97% of ε-CL (ESI, Table S6,† entry 22).

Summarizing the catalytic activity of **1–5** in the synthesis of α-hydroxy acid glyceryl esters, we found that **1** and **2** are inactive in the alcoholysis of L-LA and ε-CL. The most active in these two reactions was **5**, leading to GlL_1/GlL_2 in 120 min or $GlCL_1$ in 90 min with conversion yields of 73/24% or 97% in stoichiometry X/Gl/M = 1/2/0.02. When the catalyst concentration was increased 2.5 times in the L-LA alcoholysis reaction, the activity of **3** was almost eight times higher than that of **4**. However, in the ε-CL alcoholysis, the catalytic activity of **4** was approximately 1.3 times better than those revealed by **3**. We established that the most active one in the alcoholysis reaction of GA was **3**, leading to GlG_1 with a conversion of 20% higher than those obtained by **4** and **5** after 30 min. The presence of Al(III)/Ga(III) centers in **3** and **4** enhances their catalytic activity in GA alcoholysis compared to **5** (ESI, Table S4,† entries 14, 21 and 33). Compound **1** showed significantly greater reactivity than **2**, but GA was mainly converted to the mixture of GlG_n and GlG_2.

The ^{1}H NMR spectra of the reaction mixtures revealed the presence of glyceryl 1- and 2-lactate/glycolate/6-hydroxyhexanoate. Resonance signals from the glyceryl alkyl and hydroxyl groups were found in the same region for these compounds regardless of the units of hydroxy acids (Fig. 10 and Fig. S36, S39 in the ESI†). For example, the ^{1}H NMR spectrum presented in Fig. 10 showed resonances of glyceryl CH_2 at 4.09 and 3.94 ppm (diastereotopic protons) and 3.42 ppm; CH at 3.64 ppm, and OH at 4.89 and 4.64 ppm for glyceryl 1-lactate. The corresponding resonance signals of Gl protons in glyceryl 2-lactate were found at 4.74 ppm for CH, 3.50 for CH_2, and 3.47–3.27 for the OH groups. Resonance signals from hydroxyl, methine, and methyl protons of the lactate unit were found at 5.34, 4.14, and 1.25 ppm. Electrospray ionization mass spectrometry (ESI-MS) studies confirmed the formation of α-hydroxy acid glyceryl esters (ESI, Fig. S42–S44†).

Ring-opening polymerization of L-LA, GA, and ε-CL

The polymerization of L-LA, GA, and ε-CL was performed in THF solution or bulk using Gl as a co-initiator and compounds **1–5** as initiators to compare their catalytic activities. The amount of compound used in each reaction was calculated on the basis of the number of metal centers (M) in **1–5**. Representative results for the L-LA, GA, and ε-CL polymerizations are summarized in Table 1. The number average molecular weights (M_n) and dispersity indexes ($Đ$) of the polymers were determined by size-exclusion chromatography (SEC) with a multiangle laser-light scattering (MALLS) or refractive index detector (RI).

In the ROP of GA performed with a GA/Gl/M stoichiometry of 20/1/1, polyglycolide (PGA) formation with M_n values ranging from 13.0 to 14.9 kDa and a $Đ$ of 1.16 to 1.23 was observed. The received polymers were isolated as a crystalline precipitate after exceeding a certain molecular weight during these reactions. We suspect that the very poor solubility of the formed PGAs caused their similar M_n and $Đ$ values. Initiator **5** was the most active in GA polymerization with a GA/M ratio of 20, resulting in a monomer conversion of 99% after 1 min. Compound **3** showed a similar conversion value after 4 minutes, compound **4** after 20 minutes, and **1** after 45 minutes (Table 1, entries 1–4). When GA polymerization was performed in bulk at a GA/Gl/M = 100/1/1, the resulting PGAs had M_n values of 10.6 to 13.1 kDa and $Đ$ values within the range of 1.27 to 1.47.

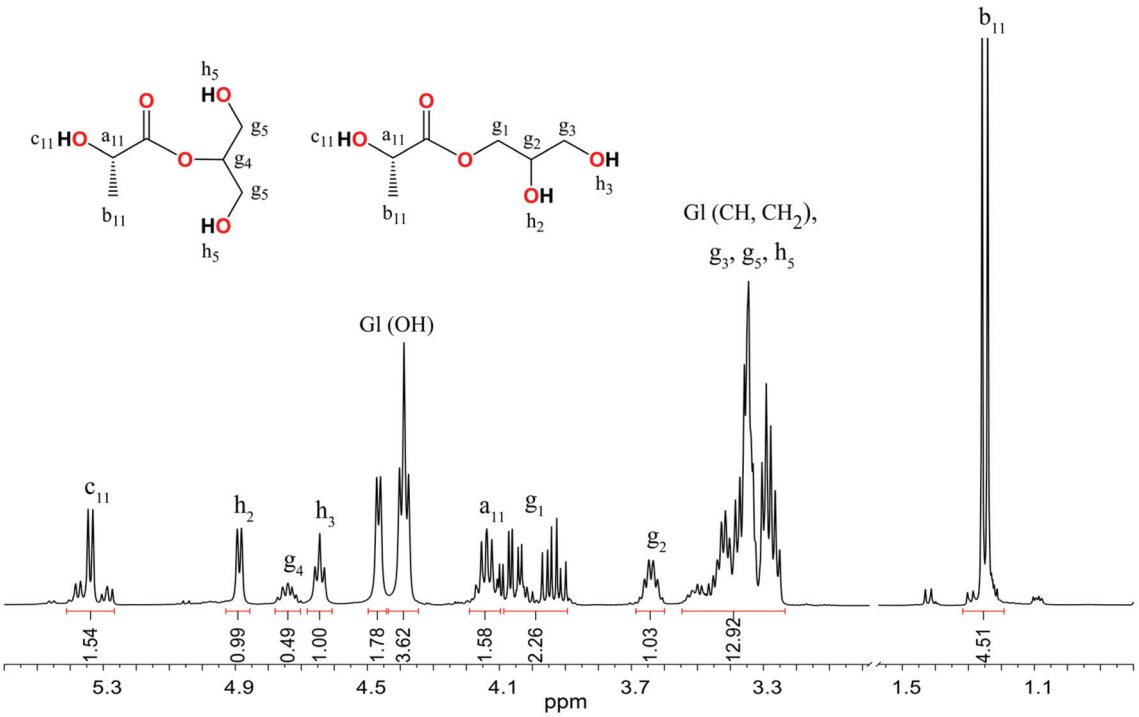

Fig. 10 ^{1}H NMR spectrum in DMSO-D_6 of GlL_1 synthesized in the L-LA alcoholysis reaction in the presence of **3**.

Table 1 Polymerization of GA, L-LA and ε-CL using **1** and **3–5** [a]

Entry	Initiator	Monomer	[X]/[Gl]/[M]	t (min)	C^b (%)	M_n [c] (kDa)	$Đ^c$	T_m [d] (°C)	T_{max} [d] (°C)
1	**1**	GA	20/1/1	93	98	13.0	1.19	191.61	317.27
2	**3**	GA	20/1/1	4	99	14.5	1.23	200.18	325.72
3	**4**	GA	20/1/1	20	99	14.9	1.15	191.18	330.44
4	**5**	GA	20/1/1	1	99	13.4	1.16	221.04	327.96
5[e]	**1**	GA	100/1/1	45	98	13.1	1.47	221.29	324.59
6[e]	**3**	GA	100/1/1	8	97	10.9	1.27	219.23	331.61
7[e]	**4**	GA	100/1/1	15	95	10.6	1.28	215.93	330.13
8[e]	**5**	GA	100/1/1	4	98	11.0	1.29	219.19	330.32
9	**1**	L-LA	20/1/1	720	76	2.9	2.90	—	275.98
10	**3**	L-LA	20/1/1	38	92	3.9	2.88	—	265.37
11	**4**	L-LA	20/1/1	300	89	9.5	2.24	—	276.17
12	**5**	L-LA	20/1/1	45	98	4.6	2.84	—	274.40
13[e]	**1**	L-LA	100/1/1	720	72	10.2	3.16	144.94	295.83
14[e]	**3**	L-LA	100/1/1	120	90	5.4	1.83	131.82	294.65
15[e]	**4**	L-LA	100/1/1	720	88	10.6	1.43	136.20	289.50
16[e]	**5**	L-LA	100/1/1	120	94	4.5	1.62	133.20	282.34
17[f]	**1**	ε-CL	200/1/1	240	82	7.0	1.80	61.31	233.72
18[f]	**3**	ε-CL	200/1/1	240	90	9.5	2.92	62.05	248.73
19[f]	**4**	ε-CL	200/1/1	240	87	9.4	2.67	61.24	246.63
20[f]	**5**	ε-CL	200/1/1	240	97	6.9	2.05	61.06	224.24

[a] Polymerization conditions: $[M]_0$ = 10 mM, 10 ml of THF as the solvent, temperature 25 °C, under an atmosphere of N_2. [b] Obtained from ^{1}H NMR analysis. [c] Obtained from SEC analysis with the RI (entries 1-8) or MALLS (entries 9-20) detector. [d] Obtained from TGA/DTA analysis; T_m – melting point; T_{max} – temperature of the maximum degradation rate. [e] GA and L-LA polymerization performed in bulk at 110 °C. [f] polymerization performed in ε-CL at 70 °C.

Compounds **1–5** were also used as initiators for the bulk polymerization of ε-CL at 70 °C with the GA/Gl/M stoichiometry of 200/1/1. After 240 min of reaction carried out with **1**, polycaprolactone (PCL) formation was observed with an M_n of 7.0 kDa and a $Đ$ of 1.80. Under the same conditions, heterometallic compounds **3–4** led to polymers with M_n values of 9.4–9.5 and $Đ$ values of 2.67–2.97 (Table 1, entries 18 and 19). The use of lithium aryloxide **5** resulted in a product with M_n = 7.2 and $Đ$ = 2.69 (Table 1, entry 20).

In the L-LA polymerization reactions, the formation of PLLAs with M_n values of 2.90 to 10.6 kDa and $Đ$ values of 1.43–3.16 was observed (Table 1, entries 9–16). When polymerization was performed with **1–5** in an L-LA/Gl/M molar ratio of 20/1/1, the M_n values of the PLLAs were 2.9 to 9.5 kDa and $Đ$ was within the range of 2.24–2.90. The most active in the ROP of L-LA was **3**, which converted 92% of the monomer in 38 min. To achieve similar results, **5** needs 45 min and **4** needs 300 min. When **1** was used for the ROP of L-LA after 720 min, 76% of the monomer conversion was achieved, and the resulting material had an M_n of 2.9 kDa and a $Đ$ of 2.9. When the ratio of L-LA/Gl/M was 100/1/1, compounds **3–5** produced polymers with M_n values of 4.5 to 10.3 kDa and $Đ$ of 1.43 to 1.83. High dispersity indices in the 1.5 to 2.9 range are typical of branched polyesters, and similar values were previously reported for 3-arm PLLAs.[100,101]

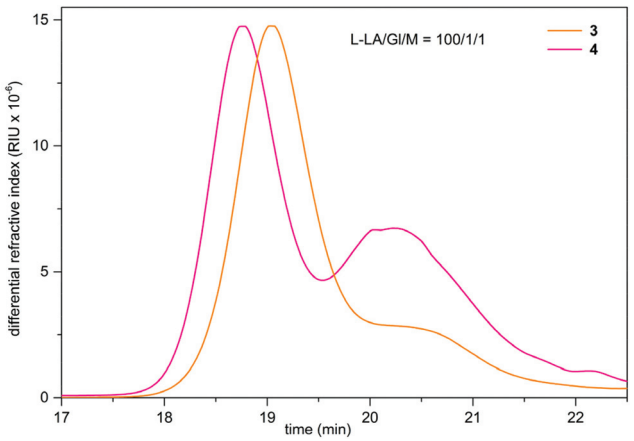

Fig. 11 SEC chromatograms of bimodal PLLAs synthesized using heterometallic **3** and **4**.

In the ROP of L-LA, the M_n and $Đ$ values of the PLLAs obtained using **3** and **5** were comparable and were at least twice lower than those synthesized with **4**. Furthermore, the SEC curves recorded for the PLLAs obtained using heterometallic **3** and **4** reveal the bimodal distribution of molecular weight. Representative SEC curves of bimodal PLLAs obtained in the presence of **3** and **4** in the reaction with L-LA/Gl/M stoichiometry of 100/1/1 are presented in Fig. 11. In these examples, the higher molecular weight fractions have estimated M_n values of 10.3 kDa with $Đ$ = 1.30 for **3** and 12.5 kDa with $Đ$ = 1.40 for **4**. The lower molecular weight fractions have M_n values of 2.3 kDa with $Đ$ = 2.13 for **3** and 8.3 kDa with $Đ$ = 1.30 for **4**. Conventionally, it is assumed that polymerization will be initiated from all functional groups using a bi- or trifunctional chain transfer agent; however, this assumption is not always substantiated.[102] We investigated the structure of the resulting PLLAs using ^{1}H-DOSY or ^{1}H–^{13}C HSQC measurements, but we did not find distinguishing signals characteristic of the formation of polymers with different architectures (ESI, Fig. S45–S48†). To exclude the possibility of the formation of different species in the solution, we performed NMR scale reactions of **3** and **4** with excess Gl, but no reaction between reagents was observed (ESI, Fig. S49 and S50†). Therefore, it is proposed that the steric hindrance and the nature of the –OH group in the chain transfer agent, the number of lithium centers in the initiator structure, and the prolonged reaction time influence the formation of the two molecular weight fractions. The sterically hindered Al(III) center in **3** is proposed to perform only a structural function, and thus only Li centers take an active part in the ROP of L-LA. Therefore, the catalytic activity of **3** is comparable to those observed for **5**. In the presence of **4**, the polymer was also proposed to be synthesized at the Li sites. However, the tetracoordinated Ga(III) center may participate in the formation of stable interactions between the carbonyl moiety of the polymer chain, and thus further acti-

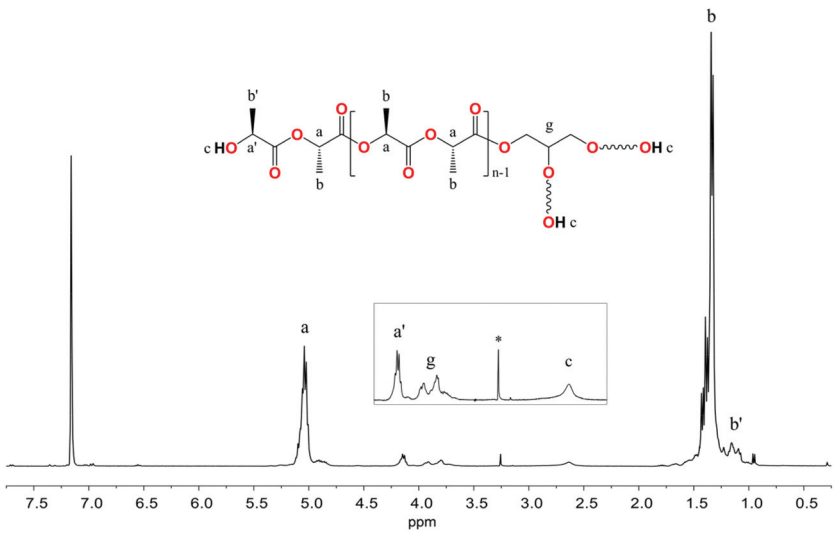

Fig. 12 ^{1}H NMR spectrum of 3-arm PLLA in C_6D_6. * – assigned ligand residues.

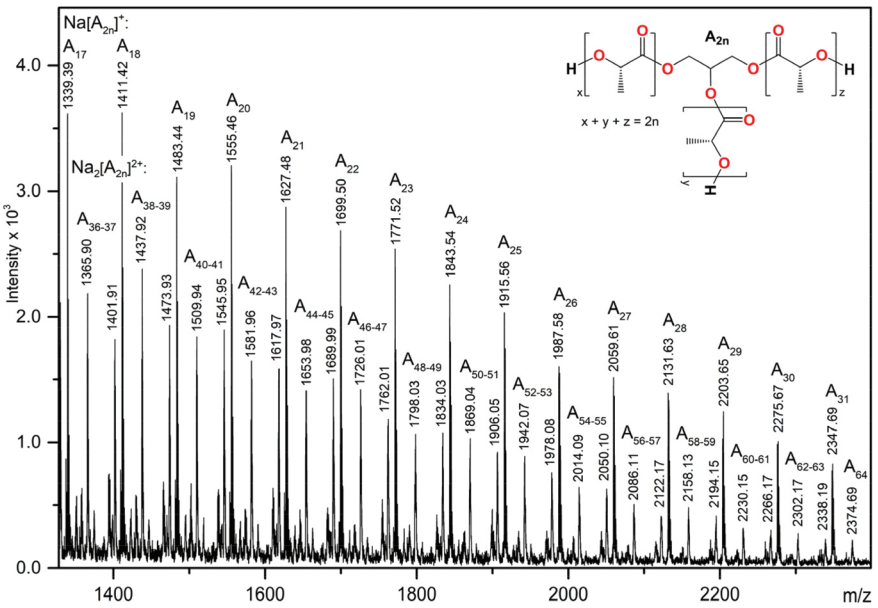

Fig. 13 Mass spectrum of 3-arm PLLA.

vation of the L-LA monomer may be limited due to the decrease in the steric accessibility of the Li center.[103] The prolonged reaction time and a temperature above 110 °C, favor the occurrence of transesterification side reactions and the formation of cyclic polymers, leading to a bimodal molecular weight distribution. These observations could also explain the reduced catalytic activity of **4** in L-LA alcoholysis, where mainly GlL_2 was synthesized despite the high content of the active lithium site (Table S4,† entries 21 and 35).

However, PCLs synthesized using heterometallic **3** and **4** have similar M_n ~9.4 kDa and $Đ$ values of 2.7–2.9 despite the different lithium center content in the initiator structure. Furthermore, both polymers have higher M_n values and broader $Đ$ than those obtained with homometallic **1** and **5**. These results suggested that multiple factors are involved in the ROP of cyclic esters, including the type of monomers used, nature and number of metallic centers, the nature and steric hindrance of the ligands, the coordination number of metal ions, and the central core structure of the initiators.

The ^{1}H NMR and ESI-MS analysis of the resulting macromolecular chain ends revealed the formation of star-shaped PGA, PLLA, or PCL with glyceryl branching points, indicating an activated monomer mechanism (Fig. 12, 13, and Fig. S51–S54 in the ESI†).[104]

For example, the ^{1}H NMR spectrum of the resulting 3-arm PLLA in C_6D_6 showed resonance signals at 4.14, 2.64, and 1.12 ppm from the CH, OH, and CH_3 groups of hydroxyl end units, the protons of the CH and CH_3 groups of the main chain at 5.06 and 1.34 ppm, and resonances for the alkyl protons of the triglyceryl ester group at 3.93 and 3.80 ppm (Fig. 12). The ESI-MS spectrum presented in Fig. 13 confirmed the formation of branched PLLAs.

Conclusion

This study developed a new, simple, and efficient strategy for the preparation of various glycerol derivatives, *i.e.*, α-hydroxy acid glyceryl esters and branched polyesters, by alcoholysis or polymerizations of L-LA, GA, and ε-CL. For these purposes, we use lithium and group 13 aryloxides $[Al(MesalO)_3]$ (**1**), $[Me_2Ga(MesalO)]_2$ (**2**), $[AlLi_3(MesalO)_6]$ (**3**), $[Me_2GaLi(MesalO)_2(THF)]$ (**4**), and $[Li_6(MesalO)_6]$ (**5**) which can play dual roles as catalysts in ester synthesis and as polymerization initiators. This approach enabled the synthesis of very attractive green chemicals that, after the implementation of a purification procedure, have the potential to be used as dietary supplements, antiseptic and antimicrobial agents, polymer additives (plasticizers, surface modification agents), or polymeric encapsulation materials. The effect of the metal aryloxide catalyst on cyclic ester alcoholysis or polymerization reactions was investigated. We showed that the type of monomers used, the nature and number of metallic centers, and the central core structure of the used initiators strongly influence the polymerization of the cyclic esters and the physicochemical properties of the resulting polymers. The first heterometallic gallium-alkali metal initiator was developed for the alcoholysis and ROP of cyclic esters. In the field of heterometallic cooperativity, we established that the presence of Al(III)/Ga(III) centers in **3** and **4** enhances the catalytic activity of active Li sites in GA alcoholysis. In the alcoholysis and polymerization of L-LA, the presence of Ga(III) decreases the catalytic activity of **4** compared to the lithium analog **5**.

Metal aryloxides **1–6** were obtained by the reaction of the ligand precursor with group 13 alkyls MMe_3 (for M = Al, Ga) or their combination with BuLi in a THF/alcohol solution. Direct

reactions of MMe_3 (for M = Al, Ga) and MesalOH (1 : 3) led to compound **1** or **2**, respectively. When the same reactions were carried out with additional BuLi, heterometallic compound **3** or the mixture of **4** and $[Li_6(MesalO)_6]$ (**5**) was obtained. In **3** and **4**, the formed group 13 species retain the rearrangements that occurred in **1** or **2**. In coordination chemistry, **3** is the second example of aryloxides with an Al : Li ratio of 1 : 3, while **4** and **6** are the fourth and fifth examples of gallium–lithium aryloxides.

Heterometallic aryloxides **3** and **4** are attractive molecular precursors for the preparation of group 13-lithium ceramics, *i.e.* γ-$LiAlO_2$ and β-$LiGaO_2$, by the thermal decomposition at 850 °C. These materials have various practical applications in coatings, battery and cell technologies, semiconductors, and laser diode fabrication.

Overall, we present new structurally authenticated group 13-lithium aryloxides, which could be helpful in the development of green chemicals, *i.e.*, α-hydroxy acid glyceryl esters or 3-arm polyesters, as well as ceramic materials of industrial importance.

Experimental section

Materials and methods

All syntheses were performed in a dry N_2 atmosphere using standard Schlenk techniques. Standard methods were used to purify the reagents: toluene, hexane, and THF were distilled over Na; CH_2Cl_2 was distilled over P_2O_5, and EtOH was distilled over Mg. All chemical reagents were purchased from commercial sources: methyl salicylate, metallic sodium, $AlMe_3$ 1.0 M in hexane, $GaMe_3$ 2.0 M in toluene, ^{n}BuLi solution 1.6 M in hexane, L-lactide, glycolide, ε-caprolactone (Sigma-Aldrich, St Louis, MO, USA); toluene, hexane, THF, CH_2Cl_2 and C_2H_5OH (POCH); CD_2Cl_2, DMSO-D_6, and THF-D_8 (Carl-Roth). L-Lactide and glycolide were recrystallized twice from toluene, sublimed, and kept over P_2O_5, andε-caprolactone was dried under vacuum and kept over molecular sieves. $AlMe_3$ and $GaMe_3$ are highly pyrophoric and should be handled and used only in an atmosphere of argon or nitrogen. The ^{1}H, ^{7}Li, and $^{13}C\{^1H\}$ NMR spectra were recorded at room temperature on a JEOL JNM-ECZ 400 MHz spectrometer. Chemical shifts were reported in parts per million and referenced to the residual protons in deuterated solvents. The ^{7}Li spectra were referenced to a 0.1 M solution of $LiNO_3$ in D_2O. FTIR-ATR spectra were recorded on a Bruker Vertex 70 vacuum spectrometer. Elemental analyses were performed on a PerkinElmer 2400 CHN elemental analyzer. Metal ion concentrations were determined by ICP-OES using a Thermo Scientific iCAP 7400 Duo spectrometer. The thermal decomposition of the metal aryloxide precursors was performed using an NT 1313 furnace (Neotherm) equipped with a KXP4 thermostat under air. The resulting metal oxide materials were investigated by powder X-ray diffraction with an Empyrean (PANalytical) diffractometer. The samples were analyzed using the PDF-4+ and COD powder diffraction database. The morphologies of the oxide materials were examined using an FEI Tecnai G^2 20 X-Twin TEM microscope equipped with a field emission gun (FEG) and an integrated energy dispersive spectrometer (EDAX). For the TEM observation, 200 mesh copper grids with lacey carbon films were used. The signals from copper and carbon (from the grids) were visible on the TEM EDX spectra. The SEC traces of PLLAs and PCLs were recorded at 30 °C with a system consisting of an Agilent 1100 Series isocratic pump, a degasser, an autosampler, a thermostatic box for columns, and a set of TSK Gel columns (2 × PLGel 5 μm MIXED-C). A Wyatt Optilab rEX interferometric refractometer and a MALLS DAWN EOS laser photometer (Wyatt Technology Corp., USA) were used as detectors. The eluent was CH_2Cl_2 with a flow rate of 0.8 ml min^{-1}. The M_n and $Đ$ values were calculated from the experimental traces using the Wyatt ASTRA v 4.90.07 program. PGA SEC traces were recorded at 40 °C with a system consisting of a SHIMADZU-LC-20AD pump, a degasser, an autosampler, a thermostatic box for columns, and a set of TSK Gel columns (2 × PLGel 5 μm MIXED-C). The RI-Optilab-T-rex-Wyatt interferometric refractometer (Wyatt Technology Corp., USA) was used as the detector. The eluent was DMF with a flow rate of 0.8 ml min^{-1}. The M_n and $Đ$ values were calculated from the experimental traces using the Wyatt ASTRA v 7.1.2 program. TGA/DSC was performed in a nitrogen atmosphere with a TGA/DSC 3+ system (Mettler-Toledo) at a heating rate of 10 °C min^{-1}.

Single-crystal X-ray diffraction studies

Single-crystal XRD data were collected using an Xcalibur Ruby, XtaLAB Synergy R, or Agilent SuperNova Dual Atlas diffractometer at 100 K for **1–4** and **6**.[105] Experimental details and crystal data are given in Table S1.† The structures were solved by direct methods and refined by the full-matrix least-squares method on F^2, using the SHELXTL package.[106] Nonhydrogen atoms were refined with anisotropic thermal parameters. All hydrogen atoms were positioned geometrically and added to the structure factor calculations but were not refined. Molecular graphics for the resulting structures were created using Diamond (version 3.1e).[107] During the single-crystal XRD measurements of **4** a higher symmetry than the real one was assumed, and only 75% of the data completeness was achieved. CCDC 2076392–2076396, 2128614 and 2128703† contain the supplementary crystallographic data for this paper.

Synthesis of $[Al(MesalO)_3]$ (1). $AlMe_3$ (3.86 ml, 3.86 mmol) was added dropwise to a solution of MesalOH (1.5 ml, 11.58 mmol) in 10 ml of THF and 20 ml of CH_3OH. The reaction mixture was then stirred at room temperature for 14 h. Then the mixture was concentrated under vacuum to half the volume and left in a refrigerator for crystallization. After several weeks, the resulting colorless plate-like crystals were filtered off, washed with hexane (3 × 10 ml), and dried under vacuum. Yield: 1.21 g (65%). Anal. Calc. for $C_{24}H_{21}O_9Al$: C, 60.00; H, 4.41. Found: C, 60.13; H, 4.43. ^{1}H NMR (400 MHz, THF-D_8): δ 7.67 (3H, tt, J = 7.9, 1.5 Hz, ArH), 7.28 (3H, t, J = 7.5 Hz, ArH), 6.63 (3H, d, J = 8.6 Hz, ArH), 6.48 (3H, t, J = 7.5

Hz, ArH), 3.79 (9H, s, CH_3). $^{13}C\{^1H\}$ NMR (101 MHz, THF-D_8): δ 174.8 (3C, C═O), 170.7 (3C, C–O), 137.6 (3C, ArH), 130.2 (3C, ArH), 123.9 (3C, ArH), 114.9 (3C, ArH), 111.5 (3C, Ar), 111.3 (3C, ArH), 53.5 (3C, CH_3). FTIR-ATR (cm^{-1}): 3058 (vw), 3035 (vw), 2956 (w), 2865 (vw), 2712 (vw), 2605 (vw), 2324 (vw), 1927 (vw), 1814 (vw), 1740 (vw), 1629 (vs), 1602 (s), 1542 (s), 1508 (vw), 1461 (s), 1440 (s), 1407 (m), 1380 (w), 1353 (s), 1303 (vw), 1267 (m), 1244 (vs), 1198 (w), 1159 (m), 1137 (m), 1094 (m), 1028 (m), 956 (w), 880 (m), 858 (m), 839 (m), 797 (m), 759 (vs), 706 (m), 669 (m), 639 (s), 572 (m), 532 (w), 462 (m), 444 (m), 419 (w), 405 (w). For catalytic purposes, the crystals of **1** were recrystallized from ethanol and, as a result of transesterification, the formation of ethyl salicylate ligands was observed.

Synthesis of [Al(EtsalO)$_3$] (1a). The synthesis was similar to the procedure described for **1**, but instead of CH_3OH, C_2H_5OH was used. The resulting block-like crystals were filtered off, washed with hexane (3 × 10 ml), and dried under vacuum. Yield: 1.13 g (56%). Anal. Calc. for $C_{27}H_{27}O_9Al$: C, 62.07; H, 5.21. Found: C, 62.11; H, 5.22. ^1H NMR (400 MHz, THF-D_8): δ 7.67 (3H, dd, J = 7.9, 1.8 Hz, ArH), 7.26 (3H, ddd, J = 8.9, 6.9, 1.8 Hz, ArH), 6.62 (3H, d, J = 8.6 Hz, ArH), 6.46 (3H, ddd, J = 7.9, 6.9, 1.2 Hz, ArH), 4.25 (6H, q, J = 7.2 Hz, CH_2), 1.25 (9H, t, J = 7.2 Hz, CH_3). $^{13}C\{^1H\}$ NMR (101 MHz, THF-D_8): δ 174.4 (3C, C═O), 170.8 (3C, C–O), 137.4 (3C, ArH), 130.2 (3C, ArH), 123.9 (3C, ArH), 114.7 (3C, ArH), 111.6 (3C, Ar), 63.4 (3C, CH_2), 14.0 (3C, CH_3). FTIR-ATR (cm^{-1}): 3092 (vw), 3034 (vw), 3009 (vw), 2983 (w), 2804 (vw), 2701 (vw), 2605 (vw), 2493 (vw), 2324 (vw), 1928 (vw), 1911 (vw), 1817 (vw), 1627 (vs), 1601 (s), 1542 (s), 1509 (vw), 1463 (s), 1450 (s), 1404 (s), 1377 (m), 1346 (s), 1301 (vw), 1267 (m), 1239 (vs), 1179 (w), 1159 (m), 1137 (m), 1094 (m), 1028 (w), 992 (w), 893 (w), 873 (vw), 859 (w), 837 (m), 800 (w), 759 (vs), 707 (m), 669 (m), 637 (s), 572 (m), 534 (w), 479 (m), 455 (m), 436 (m), 420 (w).

Synthesis of [Me$_2$Ga(MesalO)]$_2$ (2). $GaMe_3$ (1.93 ml, 3.86 mmol) was added dropwise to a solution of MesalOH (1.5 ml, 11.58 mmol) in 10 ml of THF and then 20 ml of CH_3OH was added. The reaction mixture was stirred at room temperature for 12 h, concentrated under vacuum to a volume of 3 ml, and an additional 10 ml of THF was added. Colorless plate-like crystals were grown at room temperature after 48 h. The resulting crystals were filtered off, washed with hexane (3 × 10 ml), and dried under vacuum. Compound **2** has a low melting point and could be easily purified by sublimation. Yield: 0.66 g (69%). Anal. Calc. for $C_{20}H_{26}O_6Ga_2$: C, 47.86; H, 5.22. Found: C, 47.88; H, 5.24. ^1H NMR (400 MHz, THF-D_8): δ 7.72 (2H, dd, J = 8.0, 1.4 Hz, ArH), 7.32 (2H, m, ArH), 6.73 (2H, dd, J = 8.7, 1.2 Hz, ArH), 6.55 (2H, ddd, J = 8.0, 7.0, 1.2 Hz, ArH), 3.94 (6H, s, CH_3), −0.29 (12H, s, $GaCH_3$). $^{13}C\{^1H\}$ NMR (101 MHz, THF-D_8): δ 174.6 (2C, C═O), 170.6 (2C, C–O), 137.6 (2C, ArH), 131.3 (2C, ArH), 124.2 (2C, ArH), 116.1 (2C, ArH), 112.1 (2C, Ar), 53.7 (2C, CH_3), −6.7 (4C, $GaCH_3$). FTIR-ATR (cm^{-1}): 3188 (vw), 3072 (vw), 2956 (w), 2916 (vw), 1677 (s), 1616 (m), 1586 (m), 1554 (w), 1486 (m), 1440 (s), 1327 (m), 1304 (s), 1248 (s), 1217 (vs), 1158 (m), 1136 (m), 1091 (m), 1045 (vw), 1033 (w), 964 (w), 866 (w), 849 (w), 822 (vw), 800 (vw), 753 (s), 721 (vs), 698 (vs), 666 (m), 528 (vs), 438 (m).

Synthesis of [AlLi$_3$(MesalO)$_6$] (3). $AlMe_3$ (2.57 ml, 2.57 mmol) and BuLi (3.09 ml, 7.71 mmol) were added dropwise to a solution of MesalOH (2.0 ml, 15.43 mmol) in 10 ml of THF. The reaction mixture was stirred at room temperature for 1 h, and 20 ml of CH_3OH was added. The reaction was then continued for an additional 24 h, concentrated under vacuum to half the volume, and left for crystallization. After several weeks, the resulting colorless needle-like crystals were filtered off, washed with hexane (3 × 10 ml), and dried under vacuum. Yield: 1.32 g (54%). Anal. Calc. for $C_{48}H_{42}O_{18}AlLi_3$: C, 60.39; H, 4.43; Al, 2.83; Li, 2.18. Found: C, 60.41; H, 4.44; Al, 2.85; Li, 2.16. ^1H NMR (400 MHz, THF-D_8): δ {7.68, 7.58 (6H, m, ArH)}, 7.11 (6H, m, ArH), {6.83, 6.66 (6H, m, ArH)}, {6.41, 6.29 (6H, m, ArH)}, 3.77 (12H, s, CH_3), 3.73 (6H, s, CH_3). $^{13}C\{^1H\}$ NMR (101 MHz, THF-D_8): δ 173.2–171.9 (6C, C═O), 171.1 (4C, C–O), 168.2 (2C, C–O), 135.5 (2C, ArH), 134.9 (4C, ArH), 131.8 (2C, ArH), 130.6 (4C, ArH), 124.1 (4C, ArH), 123.8 (2C, ArH), 114.9 (4C, ArH), 114.7 (2C, ArH), 112.3 (6C, Ar), 52.2 (4C, CH_3), 51.2 (2C, CH_3). ^7Li NMR (THF-D_8, 155 MHz): δ 4.00. FTIR-ATR (cm^{-1}): 3027 (vw), 2950 (w), 2844 (vw), 2319 (vw), 2234 (vw), 2162 (vw), 2141 (vw), 2109 (vw), 2081 (vw), 2049 (vw), 1979 (vw), 1925 (vw), 1703 (m), 1677 (m), 1641 (s), 1613 (vs), 1598 (vs), 1566 (w), 1546 (m), 1464 (vs), 1442 (s), 1387 (w), 1353 (m), 1325 (m), 1292 (w), 1254 (vs), 1223 (s), 1198 (m), 1153 (m), 1085 (m), 1035 (w), 954 (w), 898 (w), 861 (s), 817 (w), 798 (w), 764 (s), 755 (vs), 707 (s), 676 (w), 662 (w), 599 (m), 581(m), 558 (w), 533 (m), 493 (m), 472 (w), 451 (w), 431 (w).

Synthesis of [AlLi$_3$(EtsalO)$_6$] (3a). The synthesis was similar to the procedure described for **3**, but instead of CH_3OH, C_2H_5OH was used. The resulting block-like crystals were filtered off, washed with hexane (3 × 10 ml), and dried under vacuum. Yield: 1.68 g (63%). Anal. Calc. for $C_{54}H_{54}O_{18}AlLi_3$: C, 62.44; H, 5.24; Al, 2.60; Li, 2.00. Found: C, 62.47; H, 5.26; Al, 2.58; Li, 1.97. ^1H NMR (400 MHz, THF-D_8): δ {7.73, 7.60 (6H, m, ArH)}, 7.10 (6H, m, ArH), {6.85, 6.66 (6H, m, ArH)}, {6.41, 6.27 (6H, m, ArH)}, {4.25, 4.20 (12H, m, CH_2)}, {1.32, 1.23 (18H, m, CH_3)}. $^{13}C\{^1H\}$ NMR (101 MHz, THF-D_8): δ 173.1 (2C, C═O), 171.8 (4C, C═O), 170.6 (4C, C–O), 168.3 (2C, C–O), 135.5 (2C, ArH), 134.7 (4C, ArH), 131.8 (2C, ArH), 130.6 (4C, ArH), 124.1 (6C, ArH), 115.0 (2C, ArH), 114.9 (4C, ArH), 112.0 (6C, Ar), 61.7 (4C, CH_2), 60.2 (2C, CH_2), 14.6 (2C, CH_3), 14.3 (4C, CH_3). ^7Li NMR (THF-D_8, 155 MHz): δ 4.01. FTIR-ATR (cm^{-1}): 3072 (vw), 2982 (w), 2955 (vw), 2935 (vw), 2896 (vw), 2319 (vw), 2162 (vw), 2141 (vw), 1929 (vw), 1707 (m), 1676 (s), 1650 (s), 1620 (s), 1599 (s), 1564 (w), 1547 (m), 1467 (vs), 1445 (s), 1409 (m), 1379 (w), 1367 (w), 1342 (m), 1349 (m), 1319 (w), 1292 (m), 1255 (vs), 1230 (s), 1215 (vs), 1161 (m), 1149 (s), 1117 (vw), 1088 (s), 1076 (s), 1045 (vw), 1032 (m), 1012 (w), 952 (vw), 891 (m), 866 (m), 853 (m), 827 (m), 795 (w), 765 (vs), 758 (vs), 708 (s), 664 (m), 601 (s), 582 (m), 561(w), 534 (w), 494 (m), 476 (w), 458 (w), 425 (w), 405 (w).

Synthesis of [Me$_2$GaLi(MesalO)$_2$(THF)] (4). $GaMe_3$ (1.29 ml, 2.58 mmol) and BuLi (3.10 ml, 7.74 mmol) were added dropwise to a solution of MesalOH (2.01 ml, 15.48 mmol) in 10 ml

of THF. The reaction mixture was stirred at room temperature for 2 h, and 25 ml of CH_3OH was added. The reaction was continued for an additional 48 h, concentrated under vacuum to give colorless viscous liquids. Then 5 ml of THF was added, and the reaction mixture was left for crystallization at −28 °C. After six months, the resulting colorless plate-like crystals were filtered off and dried under vacuum. Yield: 0.94 g (25%). Anal. Calc. for $C_{22}H_{28}O_7GaLi$: C, 54.92; H, 5.87; Ga, 14.49; Li, 1.44. Found: C, 54.96; H, 5.90; Ga, 14.52; Li, 1.39. ^{1}H NMR (400 MHz, THF-D_8): δ 7.86 (2H, m, ArH), 7.28 (2H, m, ArH), 6.65 (2H, d, J = 7.9, Hz ArH), 6.60 (2H, m, ArH), 3.87 (6H, s, CH_3), 3.62 (4H, m, CH_2), 1.77 (4H, m, CH_2), −0.25 (6H, s, $GaCH_3$). $^{13}C\{^1H\}$ NMR (101 MHz, THF-D_8): δ 169.5 (2C, C═O), 166.6 (2C, C–O), 135.4 (2C, ArH), 132.5 (2C, ArH), 121.1 (2C, ArH), 116.8 (2C, Ar), 116.1 (2C, ArH), 68.0 (2C, CH_2), 51.6 (2C, CH_3), 26.2 (2C, CH_2), −6.4 (2C, $GaCH_3$). ^{7}Li NMR (THF-D_8, 155 MHz): δ 3.76. FTIR-ATR (cm^{-1}): 3363 (vw), 3059 (vw), 2952 (w), 2871 (w), 2651(vw), 2051 (vw), 1981 (vw), 1928 (vw), 1680 (vs), 1598 (m), 1561 (m), 1475 (s), 1445 (s), 1434 (s), 1317 (s), 1297 (m), 1264 (m), 1232 (vs), 1194 (m), 1160 (s), 1147 (m), 1087 (s), 1056 (m), 1044 (m), 969 (w), 953 (vw), 899 (w), 864 (m), 818 (w), 797 (w), 758 (s), 727 (m), 704 (s), 666 (m), 597 (s), 578 (s), 535 (m), 479 (m).

Synthesis of $[Li_6(MesalO)_6]$ (5). After filtering crystals of **4** into the resulting filtrate, 10 ml of toluene was added. The filtrate was then left in the refrigerator for crystallization. After several weeks of crystallization, colorless plate-like crystals of **5** were filtered off and dried under vacuum. Yield: 0.79 g (64%). Structural, spectroscopic, and analytical data for **5** have been published in ref. 108. For the catalytic study, compound **5** was synthesized according to the published procedure. Compound **5** was also isolated in the form of $[Li_6(MesalO)_6(THF)_2]$ with unit cell parameters: a = 14.448(6), b = 17.792(5), and c = 21.355(6), and α, β, γ = 90°, but the crystals were unstable due to the loss of THF, and therefore only a low-quality model was obtained.

Synthesis of $[Me_2GaLi(MesalO)_2(H_2O)]$ (6). The crystals of **4** were left overnight under an air atmosphere, and after 12 h the crystals of **6** were obtained.

Cyclic esters' alcoholysis procedure. The typical alcoholysis procedure for synthesizing glyceryl lactate, glyceryl glycolate, or glyceryl 6-hydroxyhexanoate is as follows. For catalyst-free reactions, GA (1.22 g, 10.5 mmol), L-LA (1.51 g, 10.5mmol) or ε-CL (1.16 ml, 10.5 mmol) was added to 20 ml of THF and 0.77, 1.54, or 2.31 ml of glycerol in a stoichiometry of L-LA, GA, ε-CL/Gl = 1/1–3 (ESI, Tables S2 and S3†). For the alcoholysis reactions of cyclic esters carried out in the presence of catalyst sources, a solution of **1–5** in 1 ml of THF was added to a solution of GA/L-LA/ε-CL (4.24 mmol) and glycerol (8.48, 12.72 mmol) in 7 ml of THF at a stoichiometry of GA, L-LA, ε-CL/Gl/M = 1/2–3/0.01–0.02 (ESI, Tables S4–S6†). The reaction mixture was stirred for the prescribed time. Then, THF was removed under vacuum, and the conversion yields of α-hydroxy acid glyceryl esters were determined by ^{1}H NMR spectroscopy.

Glyceryl (*S*,*S*)-*O*-lactyllactate (GlL_2)

Glyceryl 1-((*S*,*S*)-*O*-lactyllactate). ^{1}H NMR (DMSO-D_6, 400 MHz): δ 5.45 (d, J = 5.8 Hz, 1H, HO(CHC═O)), 5.05 (q, J = 7.0 Hz, 1H, CH(C═O)), 4.92 (dd, J = 5.2, 3.4 Hz, 1H, HO(CH)), 4.65 (m, 1H, $HO(CH_2)$), 4.20 (m, 1H, CH(C═O)), 4.08, 3.95 (m, 2H, OCH_2), 3.64 (m, 1H, CH(OH)), 3.42 (m, 2H, $CH_2(OH)$), 1.42 (d, J = 7.0 Hz, 3H, $CH_3(CHO)$), 1.30 (d, J = 7.0 Hz, 3H, $CH_3(CHOH)$). $^{13}C\{^1H\}$ NMR (DMSO-D_6, 101 MHz): δ 174.1 (1C, C═O), 170.3 (1C, C═O), 72.5 (1C, $CH_2(OH)$), 69.2 (1C, CH(OH)), 68.3 (1C, CH(C═O)), 65.6 (1C, CH(C═O)), 66.4 (1C, OCH_2), 20.4 (1C, $CH_3(CHOH)$), 16.7 (1C, $CH_3(CHO)$).

Glyceryl 2-((*S*,*S*)-*O*-lactyllactate). ^{1}H NMR (DMSO-D_6, 400 MHz): δ 5.45 (d, J = 5.8 Hz, 1H, HO(CHC═O)), 5.05 (q, J = 7.0 Hz, 1H, CH(C═O)), 4.74 (m, 1H, OCH), 4.20 (m, 1H, CH(C═O)), 3.49 (m, 4H, $CH_2(OH)$), 3.47–3.24 (s, 2H, $HO(CH_2)$), 1.42 (d, J = 7.0 Hz, 3H, $CH_3(CHO)$), 1.30 (d, J = 7.0 Hz, 3H, $CH_3(CHOH)$). $^{13}C\{^1H\}$ NMR (DMSO-D_6, 101 MHz): δ 174.1 (1C, C═O), 170.3 (1C, C═O), 76.6 (1C, OCH), 68.3 (1C, CH(C═O)), 65.6 (1C, CH(C═O)), 59.5 (2C, $CH_2(OH)$), 20.4 (1C, $CH_3(CHOH)$), 16.7 (1C, $CH_3(CHO)$).

Glyceryl glycolylglycolate (GlG_2)

Glyceryl 1-glycolylglycolate. ^{1}H NMR (DMSO-D_6, 400 MHz): δ 5.49 (m, 1H, $HO(CH_2C═O)$), 4.97 (d, J = 5.2 Hz, 1H, HO(CH)), 4.71 (s, 2H, $CH_2(C═O)$), 4.69 (t, J = 5.7 Hz, 1H, $HO(CH_2)$), 4.14, 3.98 (m, 2H, OCH_2), 4.11 (m, 2H, $CH_2(C═O)$), 3.66 (m, 1H, CH(OH)), 3.49 (m, 2H, $CH_2(OH)$). $^{13}C\{^1H\}$ NMR (DMSO-D_6, 101 MHz): δ 172.3 (1C, C═O), 167.8 (1C, C═O), 72.3 (1C, $CH_2(OH)$), 69.2 (1C, CH(OH)), 66.2 (1C, OCH_2), 60.4 (1C, $CH_2(C═O)$), 59.4 (1C, $CH_2(C═O)$).

Glyceryl 2-glycolylglycolate. ^{1}H NMR (DMSO-D_6, 400 MHz): δ 5.49 (m, 1H, $HO(CH_2C═O)$), 4.89 (m, 1H, OCH), 4.70 (s, 2H, $CH_2(C═O)$), 4.11 (m, 2H, $CH_2(C═O)$, 3.54–3.45 (m, 4H, $CH_2(OH)$), 3.45–3.24 (s, 2H, $HO(CH_2)$).

Glyceryl tris(glycolyl)glycolate (GlG_4)

Glyceryl 1-tris(glycolyl)glycolate. ^{1}H NMR (DMSO-D_6, 400 MHz): δ 5.52 (m, 1H, $HO(CH_2C═O)$), 4.97 (d, J = 5.2 Hz, 1H, HO(CH)), 4.88 (s, 2H, $CH_2(C═O)$), 4.83 (s, 2H, $CH_2(C═O)$), 4.78 (s, 2H, $CH_2(C═O)$), 4.69 (t, J = 5.7 Hz, 1H, $HO(CH_2)$), 4.14, 3.98 (m, 2H, OCH_2), 4.11 (m, 2H, $CH_2(C═O)$), 3.66 (m, 1H, CH(OH)), 3.49 (m, 2H, $CH_2(OH)$).

Glyceryl 2-tris(glycolyl)glycolate. ^{1}H NMR (DMSO-D_6, 400 MHz): δ 5.52 (m, 1H, $HO(CH_2C═O)$), 4.89 (m, 1H, OCH), 4.88 (s, 2H, $CH_2(C═O)$), 4.83 (s, 2H, $CH_2(C═O)$), 4.78 (s, 2H, $CH_2(C═O)$), 4.11 (m, 2H, $CH_2(C═O)$), 3.54–3.45 (m, 4H, $CH_2(OH)$), 3.45–3.24 (s, 2H, $HO(CH_2)$).

Glyceryl (*S*)-lactate (GlL_1)

Glyceryl 1-((*S*)-lactate). ^{1}H NMR (DMSO-D_6, 400 MHz): δ 5.34 (d, J = 5.8 Hz, 1H, HO(CH C═O)), 4.89 (d, J = 5.4 Hz, 1H, HO(CH)), 4.64 (t, J = 5.5 Hz, 1H, $HO(CH_2)$), 4.14 (m, 1H, CH(C═O)), 4.09, 3.94 (m, 2H, OCH_2), 3.64 (m, 1H, CH(OH)), 3.42 (m, 2H, $CH_2(OH)$), 1.25 (d, J = 6.7 Hz, 3H, CH_3). $^{13}C\{^1H\}$ NMR (DMSO-D_6, 101 MHz): δ 174.7 (1C, C═O), 72.5 (1C, $CH_2(OH)$),

69.3 (1C, CH(OH)), 66.0 (1C, CH(C═O)), 65.7 (1C, OCH_2), 20.5 (1C, CH_3).

Glyceryl 2-((*S*)-lactate). ^{1}H NMR (DMSO-D_6, 400 MHz): δ 5.34 (d, J = 5.8 Hz, 1H, HO(CH C═O)), 4.74 (m, 1H, OCH), 4.14 (m, 1H, CH(C═O)), 3.50 (m, 4H, CH_2(OH)), 3.47–3.24 (s, 2H, HO(CH_2)), 1.25 (d, J = 6.7 Hz, 3H, CH_3). ^{13}C{^{1}H} NMR (DMSO-D_6, 101 MHz): δ 174.5 (1C, C═O), 75.8 (1C, OCH), 66.0 (1C, CH (C═O)), 59.8 (2C, CH_2(OH)), 20.6 (1C, CH_3).

Glyceryl glycolate (GlG_1)

Glyceryl 1-glycolate. ^{1}H NMR (DMSO-D_6, 400 MHz): δ 5.29 (m, 1H, HO(CH_2C═O)), 4.89 (d, J = 5.5 Hz, 1H, HO(CH)), 4.64 (t, J = 5.5 Hz, 1H, HO(CH_2)), 4.09, 3.94 (m, 2H, OCH_2), 4.01 (m, 2H, CH_2(C═O)), 3.64 (m, 1H, CH(OH)), 3.42 (m, 2H, CH_2(OH)). ^{13}C{^{1}H} NMR (DMSO-D_6, 101 MHz): δ 172.8 (1C, C═O), 72.6 (1C, CH_2(OH)), 69.3 (1C, CH(OH)), 65.7 (1C, OCH_2), 59.7 (1C, CH_2(C═O)).

Glyceryl 2-glycolate. ^{1}H NMR (DMSO-D_6, 400 MHz): δ 5.29 (m, 1H, HO(CH_2C═O)), 4.76 (m, 1H, OCH), 4.01 (m, 2H, CH_2(C═O), 3.49 (m, 4H, CH_2(OH)), 3.45–3.24 (s, 2H, HO(CH_2)). ^{13}C{^{1}H} NMR (DMSO-D_6, 101 MHz): δ 172.6 (1C, C═O), 75.9 (1C, OCH), 59.8 (2C, CH_2(OH)), 59.6 (1C, CH_2(C═O)).

Glyceryl 6-hydroxyhexanoate ($GlCL_1$)

Glyceryl 1-(6-hydroxyhexanoate). ^{1}H NMR (DMSO-D_6, 400 MHz): δ 4.86 (d, J = 5.4 Hz, 1H, HO(CH)), 4.63 (t, J = 5.5 Hz, 1H, HO(CH_2)), 4.35 (m, 1H, HO(CH_2)$_5$), 3.96 (ddd, J = 17.7, 11.2, 5.4 Hz, 2H, OCH_2), 3.62 (m, 1H, CH(OH)), 3.42 (m, 2H, CH_2(OH)), 3.36 (m, 2H, CH_2(CH_2)$_4$C═O), 2.29 (m, 2H, CH_2(C═O)), 1.52 (m, 2H, CH_2(CH_2C═O)), 1.40 (m, 2H, CH_2(CH_2OH)), 1.28 (m, 2H, CH_2(CH_2CH_2OH)). ^{13}C{^{1}H} NMR (DMSO-D_6, 101 MHz): δ 173.0 (1C, C═O), 72.5 (1C, CH_2(OH)), 69.3 (1C, CH(OH)), 65.5 (1C, OCH_2), 59.8 (1C, CH_2(CH_2)$_4$C═O), 33.6 (1C, CH_2(CO), 32.2 (1C, CH_2(CH_2OH)), 25.1 (1C, CH_2(CH_2CH_2OH)), 24.4 (1C, CH_2(CH_2C═O)).

Glyceryl 2-(6-hydroxyhexanoate). ^{1}H NMR (DMSO-D_6, 400 MHz): δ 4.72 (m, 1H, OCH), 4.35 (m, 1H, HO(CH_2)$_5$), 3.48 (m, 4H, CH_2(OH)), 3.36 (m, 2H, CH_2(CH_2)$_4$C═O), 3.40–3.23 (s, 2H, HO(CH_2)), 2.29 (m, 2H, CH_2(C═O)), 1.52 (m, 2H, CH_2(CH_2C═O)), 1.40 (m, 2H, CH_2(CH_2OH)), 1.28 (m, 2H, CH_2(CH_2CH_2OH)). ^{13}C{^{1}H} NMR (DMSO-D_6, 101 MHz): δ 173.0 (1C, C═O), 75.4 (1C, OCH), 60.5 (2C, CH_2OH), 59.8 (1C, CH_2(CH_2)$_4$C═O), 33.6 (1C, CH_2(C═O), 32.2 (1C, CH_2(CH_2OH)), 25.1 (1C, CH_2(CH_2CH_2OH)), 24.4 (1C, CH_2(CH_2C═O)).

Cyclic esters' polymerization procedure. The typical cyclic ester polymerization procedure for PGA, PLLA, or PCL synthesis is as follows. A mixture of glycerol (7.64 μL, 0.1 mmol) and an appropriate amount of **1–5** calculated based on the number of metal centers M (0.1 mmol) in 1 ml of THF were added to a solution of L-LA, GA, and ε-CL in THF (9 ml) at a stoichiometry of [GA, L-LA, ε-CL]/[Gl]/[M] = 20/1/1 (Table 1, entries 1–4 and 9–12). For bulk GA and L-LA polymerizations, the initiators **1–5** and Gl (7.64 μL, 0.1 mmol) were introduced to the melted monomer at 110 °C or into liquid ε-CL at 70 °C at a stoichiometry of [GA, L-LA, ε-CL]/[Gl]/[M] = 100 or 200/1/1 (Table 1, entries 5–8 and 13–20). The reaction mixtures were stirred for the prescribed time. The conversion yields of the polymers were determined by ^{1}H NMR spectroscopy. The resulting PLLAs and PCLs were dissolved in CH_2Cl_2, and the reactions were quenched with cold methanol. The PGAs were dissolved in DMF and then quenched with methanol. The polymers were filtered off and dried under vacuum.

Author contributions

Rafał Petrus: involved in conceptualization, investigation, project administration, funding acquisition, and original draft writing and editing. Józef Utko: crystallization of **1**, **3** and **3a**. Joanna Petrus: IR investigations of **1–6** and writing – original draft. Mohammad Awashra: the study of L-LA and GA alcoholysis under catalyst-free conditions or using **5**. Tadeusz Lis: single-crystal X-ray diffraction measurements of **1–3a** and **6**. All authors have read and approved the final version of the manuscript.

Conflicts of interest

There are no conflicts to declare.

Acknowledgements

We thank the Polish National Science Center for financial support, grant number 2017/26/D/ST5/01123.

Notes and references

1 K. A. Wurzel, Glycerol, in *Encyclopedia of Toxicology*, ed. P. Wexler, Elsevier, 2nd edn, 2005, pp. 449–451.
2 H. W. Tan, A. A. A. Raman and M. K. Aroua, Glycerol Production and Its Applications as a Raw Material: A Review, *Renewable Sustainable Energy Rev.*, 2013, **27**, 118–127.
3 Y. Wang, J. Zhou and X. Guo, Catalytic Hydrogenolysis of Glycerol to Propanediols: A Review, *RSC Adv.*, 2015, **5**(91), 74611–74628.
4 X.-L. Li, Q. Zhou, S.-X. Pan, Y. He and F. Chang, A Review of Catalytic Upgrading of Biodiesel Waste Glycerol to Valuable Products, *Curr. Green Chem.*, 2020, **7**(3), 259–266.
5 S. Sahani, S. N. Upadhyay and Y. C. Sharma, Critical Review on Production of Glycerol Carbonate from Byproduct Glycerol through Transesterification, *Ind. Eng. Chem. Res.*, 2021, **60**(1), 67–88.
6 A. G. Adeniyi and J. O. Ighalo, A Review of Steam Reforming of Glycerol, *Chem. Pap.*, 2019, **73**(11), 2619–2635.
7 S. Veluturla, N. Archna, D. S. Rao, N. Hezil, I. S. Indraja and S. Spoorthi, Catalytic Valorization of Raw Glycerol

Derived from Biodiesel: A Review, *Biofuels*, 2018, **9**(3), 305–314.

8 Y. Wang, S. Lu, P. Gabriele and J. J. Harris, Poly(Glycerol Sebacate) in Tissue Engineering and Regenerative Medicine, *Mater. Matters*, 2016, **11**(3), 80–83.

9 A. M. Fischer, C. Schüll and H. Frey, Hyperbranched Poly (Glycolide) Copolymers with Glycerol Branching Points via Ring-Opening Copolymerization, *Polymer*, 2015, **72**, 436–446.

10 F. K. Wolf, A. M. Fischer and H. Frey, Poly(Glycolide) Multi-Arm Star Polymers: Improved Solubility via Limited Arm Length, *Beilstein J. Org. Chem.*, 2010, **6**, 67.

11 E. Göktürk, A. G. Pemba and S. A. Miller, Polyglycolic Acid from the Direct Polymerization of Renewable C1 Feedstocks, *Polym. Chem.*, 2015, **6**(21), 3918–3925.

12 A. Michalski, M. Brzezinski, G. Lapienis and T. Biela, Star-Shaped and Branched Polylactides: Synthesis, Characterization, and Properties, *Prog. Polym. Sci.*, 2019, **89**, 159–212.

13 M. Ghasri, A. Jahandideh, K. Kabiri, H. Bouhendi, M. J. Zohuriaan-Mehr and N. Moini, Glycerol-Lactic Acid Star-Shaped Oligomers as Efficient Biobased Surface Modifiers for Improving Superabsorbent Polymer Hydrogels, *Polym. Adv. Technol.*, 2019, **30**(2), 390–399.

14 G. A. Brooks, Glycerol-Lactate Esters for Use as an Energy Supplement during Exercise and Recovery, US6743821B2, 2004. SciFinder Scholar 2008:23397.

15 D. H. Bae and G. E. Lee, Antiseptic and Antibacterial Composition for External Application, Containing Glycerin Lactic Acid Ester as Active Ingredient, WO2018048042A11, 2018. SciFinder Scholar 2018:444780.

16 Y. Yuan, Z. Hu, X. Fu, L. Jiang, Y. Xiao, K. Hu, P. Yan and J. Lei, Poly(Lactic Acid) Plasticized by Biodegradable Glyceryl Lactate, *J. Appl. Polym. Sci.*, 2016, **133**(21), 43460.

17 H.-J. Jung, Y. Cho, D. Kim and P. Mehrkhodavandi, Cationic Aluminum, Gallium, and Indium Complexes in Catalysis, *Catal. Sci. Technol.*, 2021, **11**(1), 62–91.

18 S. Saito and H. Yamamoto, Designer Lewis Acid Catalysts —Bulky Aluminium Reagents for Selective Organic Synthesis, *Chem. Commun.*, 1997, **17**, 1585–1592.

19 S. Saito, Aluminum Trisphenoxide Polymer as a Lewis Acidic, Solid Catalyst, *Synlett*, 1999, (1), 57–58.

20 D. Tanaka, Y. Kadonaga, Y. Manabe, K. Fukase, S. Sasaya, H. Maruyama, S. Nishimura, M. Yanagihara, A. Konishi and M. Yasuda, Synthesis of Cage-Shaped Aluminum Aryloxides: Efficient Lewis Acid Catalyst for Stereoselective Glycosylation Driven by Flexible Shift of Four- to Five-Coordination, *J. Am. Chem. Soc.*, 2019, **141**(44), 17466–17471.

21 X.-X. Zheng and Z.-X. Wang, Synthesis of Aluminum Complexes Supported by 2-(1,10-Phenanthrolin-2-Yl) Phenolate Ligands and Their Catalysis in the Ring-Opening Polymerization of Cyclic Esters, *RSC Adv.*, 2017, **7**(44), 27177–27188.

22 C. Zhang and Z.-X. Wang, Aluminum and Zinc Complexes Supported by Functionalized Phenolate Ligands: Synthesis, Characterization and Catalysis in the Ring-Opening Polymerization of ε-Caprolactone and Rac-Lactide, *J. Organomet. Chem.*, 2008, **693**(19), 3151–3158.

23 A. M. McCollum, A. M. Longo, A. E. Stahl, A. S. Butler, A. L. Rheingold, T. R. Cundari, D. B. Green, K. R. Brereton and J. M. Fritsch, Synthesis, Spectroscopy, and Crystallography of Mononuclear, Five-Coordinate Aluminum Complexes That Act as Cyclic Ester Polymerization Initiators, *Polyhedron*, 2021, **204**(115233), 115233.

24 B. Gao, D. Li, Y. Li, Q. Duan, R. Duan and X. Pang, Ring-Opening Polymerization of Lactide Using Chiral Salen Aluminum Complexes as Initiators: High Productivity and Stereoselectivity, *New J. Chem.*, 2015, **39**(6), 4670–4675.

25 Y. Chapurina, T. Roisnel, J.-F. Carpentier and E. Kirillov, Zinc, Aluminum and Group 3 Metal Complexes of Sterically Demanding Naphthoxy-Pyridine Ligands: Synthesis, Structure, and Use in ROP of Racemic Lactide and β-Butyrolactone, *Inorg. Chim. Acta*, 2015, **431**, 161–175.

26 L. Qin, Y. Zhang, J. Chao, J. Cheng and X. Chen, Four- and Five-Coordinate Aluminum Complexes Supported by N, O-Bidentate β-Pyrazylenolate Ligands: Synthesis, Structure and Application in ROP of ε-Caprolactone and Lactide, *Dalton Trans.*, 2019, **48**(32), 12315–12325.

27 C. Robert, T. E. Schmid, V. Richard, P. Haquette, S. K. Raman, M.-N. Rager, R. M. Gauvin, Y. Morin, X. Trivelli, V. Guérineau, I. del Rosal, L. Maron and C. M. Thomas, Mechanistic Aspects of the Polymerization of Lactide Using a Highly Efficient Aluminum(III) Catalytic System, *J. Am. Chem. Soc.*, 2017, **139**(17), 6217–6225.

28 K. Nie, C. Wang, X. Cheng, J. Li, Y. Han and Y. Yao, Unbridged bidentate aluminum complexes supported by diaroylhydrazone ligands: Synthesis, structure and catalysis in polymerization of ε-caprolactone and lactides, *Appl. Organomet. Chem.*, 2020, **34**, e5627.

29 E. Yue, F. Cao, J. Zhang, W. Zhang, Y. Jiang, T. Liang and W.-H. Sun, Bimetallic Aluminum Complexes Bearing Novel Spiro-Phenanthrene-Monoketone/OH Derivatives: Synthesis, Characterization and the Ring-Opening Polymerization of ε-Caprolactone, *RSC Adv.*, 2021, **11**(22), 13274–13281.

30 F. Isnard, F. Santulli, M. Cozzolino, M. Lamberti, C. Pellecchia and M. Mazzeo, Tetracoordinate Aluminum Complexes Bearing Phenoxy-Based Ligands as Catalysts for Epoxide/Anhydride Copolymerization: Some Mechanistic Insights, *Catal. Sci. Technol.*, 2019, **9**(12), 3090–3098.

31 N. Zhao, Q. Wang, G. Hou, H. Song and G. Zi, Synthesis, Structure, and Catalytic Activity of Aluminum Chloride Complexes with Chiral Biaryl Schiff-Base Ligands, *Inorg. Chem. Commun.*, 2014, **44**, 86–90.

32 D. Specklin, C. Fliedel, F. Hild, S. Mameri, L. Karmazin, C. Bailly and S. Dagorne, Mononuclear Salen-Gallium Complexes for Iso-Selective Ring-Opening Polymerization

(ROP) of Rac-Lactide, *Dalton Trans.*, 2017, **46**(38), 12824–12834.

33 M. T. Muñoz, M. Palenzuela, T. Cuenca and M. E. G. Mosquera, Aluminum Aryloxide Compounds as Very Active Catalysts for Glycidyl Methacrylate Selective Ring-Opening Polymerization, *ChemCatChem*, 2018, **10**(5), 936–939.

34 H. Sasai, T. Arai, Y. Satow, K. N. Houk and M. Shibasaki, The First Heterobimetallic Multifunctional Asymmetric Catalyst, *J. Am. Chem. Soc.*, 1995, **117**(23), 6194–6198.

35 W. Gruszka, A. Lykkeberg, G. S. Nichol, M. P. Shaver, A. Buchard and J. A. Garden, Combining Alkali Metals and Zinc to Harness Heterometallic Cooperativity in Cyclic Ester Ring-Opening Polymerisation, *Chem. Sci.*, 2020, **11**(43), 11785–11790.

36 R. Petrus, J. Utko, R. Gniłka, M. G. Fleszar, T. Lis and P. Sobota, Solvothermal Alcoholysis Method for Recycling High-Consistency Silicone Rubber Waste, *Macromolecules*, 2021, **54**(5), 2449–2465.

37 R. E. Mulvey, F. Mongin, M. Uchiyama and Y. Kondo, Deprotonative Metalation Using Ate Compounds: Synergy, Synthesis, and Structure Building, *Angew. Chem., Int. Ed.*, 2007, **46**, 3802–3824.

38 W. Gruszka, H. Sha, A. Buchard and J. A. Garden, Heterometallic cooperativity in divalent metal ProPhenol catalysts: combining zinc with magnesium or calcium for cyclic ester ringopening polymerisation, *Catal. Sci. Technol.*, 2022, DOI: 10.1039/d1cy01914g.

39 T. Arai, H. Sasai, K.-I. Aoe, K. Okamura, T. Date and M. Shibasaki, A New Multifunctional Heterobimetallic Asymmetric Catalyst for Michael Additions and Tandem Michael–Aldol Reactions, *Angew. Chem., Int. Ed. Engl.*, 1996, **35**(1), 104–106.

40 T. Arai, H. Sasai, K. Yamaguchi and M. Shibasaki, Regioselective Catalytic Asymmetric Reaction of Horner-Wadsworth-Emmons Reagents with Enones: The Odyssey of Chiral Aluminum Catalysts, *J. Am. Chem. Soc.*, 1998, **120**, 441–442.

41 S. Matsunaga, J. Das, J. Roels, E. M. Vogl, N. Yamamoto, T. Iida, K. Yamaguchi and M. Shibasaki, Catalytic Enantioselective Meso-Epoxide Ring Opening Reaction with Phenolic Oxygen Nucleophile Promoted by Gallium Heterobimetallic Multifunctional Complexes, *J. Am. Chem. Soc.*, 2000, **122**(10), 2252–2260.

42 W. Gruszka and J. A. Garden, Advances in heterometallic ring-opening (co)polymerisation catalysis, *Nat. Commun.*, 2021, **12**, 3252.

43 F. Hild, P. Haquette, L. Brelot and S. Dagorne, Synthesis and structural characterization of well-defined anionic aluminium alkoxide complexes supported by NON-type diamido ether tridentate ligands and their use for the controlled ROP of lactide, *Dalton Trans.*, 2010, **39**, 533–540.

44 T. Muñoz, T. Cuenca and M. E. G. Mosquera, Heterometallic aluminates: alkali metals trapped by an aluminium aryloxide claw, *Dalton Trans.*, 2014, **43**, 14377–14385.

45 M. Normand, E. Kirillov, T. Roisnel and J.-F. Carpentier, Indium Complexes of Fluorinated Dialkoxy-Diimino Salen-like Ligands for Ring Opening Polymerization of rac-Lactide: How Does Indium Compare to Aluminum?, *Organometallics*, 2012, **31**, 1448–1457.

46 W. T. Diment, G. L. Gregory, R. W. F. Kerr, A. Phanopoulos, A. Buchard and C. K. Williams, Catalytic Synergy Using Al(III) and Group 1 Metals to Accelerate Epoxide and Anhydride Ring-Opening Copolymerizations, *ACS Catal.*, 2021, **11**, 12532–12542.

47 S. W. Kwon and S. B. Park, Effect of precursors on the morphology of lithium aluminate prepared by hydrothermal treatment, *J. Mater. Sci.*, 2000, **35**, 1973–1978.

48 O. Renoult, J.-P. Boilot and M. Boncoeur, Alkoxide-Hydroxide Route for the Preparation of γ-$LiAlO_2$-Based Ceramics, *J. Nucl. Mater.*, 1995, **26**, 233–239.

49 F. Bianchini, H. Fjellvåg and P. Vajeeston, A First Principle Comparative Study of the Ionic Diffusivity in $LiAlO_2$ and $NaAlO_2$ Polymorphs for Solid-State Battery Applications, *Phys. Chem. Chem. Phys.*, 2018, **20**(15), 9824–9832.

50 E. Temeche, S. Indris and R. M. Laine, $LiAlO_2$/$LiAl_5O_8$ Membranes Derived from Flame-Synthesized Nanopowders as a Potential Electrolyte and Coating Material for All-Solid-State Batteries, *ACS Appl. Mater. Interfaces*, 2020, **12**(41), 46119–46131.

51 R. Baron, T. Wejrzanowski, J. Milewski, Ł. Szabłowski, A. Szczęśniak and K.-Z. Fung, Manufacturing of γ-LiAlO2 Matrix for Molten Carbonate Fuel Cell by High-Energy Milling, *Int. J. Hydrogen Energy*, 2018, **43**(13), 6696–6700.

52 S. W. Kwon and S. B. Park, Effect of Precursors on the Preparation of Lithium Aluminate, *J. Nucl. Mater.*, 1997, **246**(2–3), 131–138.

53 C. Chen, C.-A. Li, S.-H. Yu and M. M. C. Chou, Growth and Characterization of β-$LiGaO_2$ Single Crystal, *J. Cryst. Growth*, 2014, **402**, 325–329.

54 L. Trinkler, A. Trukhin, B. Berzina, V. Korsaks, P. Ščajev, R. Nedzinskas, S. Tumėnas, M. M. C. Chou, L. Chang and C.-A. Li, Luminescence Properties of $LiGaO_2$ Crystal, *Opt. Mater.*, 2017, **69**, 449–459.

55 E. S. Hellman, Z. Liliental-Weber and D. N. E. Buchanan, Epitaxial Growth and Orientation of GaN on (1 0 0) γ-LiAlO2, *MRS Internet J. Nitride Semicond. Res.*, 1997, **2**, 32.

56 C. Chen, S. Sun, M. M. C. Chou and K. Xie, In Situ Inward Epitaxial Growth of Bulk Macroporous Single Crystals, *Nat. Commun.*, 2017, **8**, 2178.

57 J. Wang, L. Pu, G. Tang and J. Zhang, Electronic and Structural Characterization of InN Heterostructures Grown on β-LiGaO2 (001) Substrates, *Vacuum*, 2015, **119**, 106–111.

58 C. Chen, T. Yan, S.-H. Yu, C.-Y. Lee, C.-W. Chang and M. M. C. Chou, Microstructural and Optical Properties of High-Quality ZnO Epitaxially Grown on a LiGaO2 Substrate, *RSC Adv.*, 2015, **5**(45), 35405–35411.

59 T. Yan, Y. Min, M. Lin, C. Chen, C. Lee, L. Zhao, N. Ye, M. M. C. Chou, H. Liu and W. Zhou, Intersected Nonpolar

ZnO Nanosail Arrays Aligned Epitaxially on LiGaO2 Substrate towards Enhanced Photoelectrochemical Responses, *Nano Sel.*, 2021, **2**(6), 1233–1243.

60 J. Lewiński, J. Zachara and E. Grabska, Synthesis and Molecular Structure of (tBuOO)(tBuO)Al(μ-OtBu)2Al (mesal)2. The First Structurally Characterized (Alkylperoxo)aluminum Compound, *J. Am. Chem. Soc.*, 1996, **118**(28), 6794–6795.

61 S. Dutta and V. Manivannan, A Mononuclear Manganese (III) Schiff Base Complex, $[Mn(C_{14}H_{10}N_2O_2)(C_8H_7O_3)(CH_4O)]$, *Acta Crystallogr., Sect. C: Cryst. Struct. Commun.*, 1995, **51**, 813–815.

62 F. E. Jacobsen and S. M. Cohen, Using Model Complexes To Augment and Advance Metalloproteinase Inhibitor Design, *Inorg. Chem.*, 2004, **43**, 3038–3047.

63 L. M. R. Hill, M. K. Taylor, V. W. L. Ng and C. G. Young, Toward Multifunctional Mo(VI–IV) Complexes: cis-Dioxomolybdenum(VI) Complexes Containing Hydrogen-Bond Acceptors or Donors, *Inorg. Chem.*, 2008, **47**, 1044–1052.

64 T. Ohta, T. Imagawa and S. Ito, Involvement of transient receptor potential vanilloid subtype 1 in analgesic action of methylsalicylate, *Mol. Pharmacol.*, 2009, **75**, 307–317.

65 A. Lapczynski, L. Jones, D. McGinty, S. P. Bhatia, C. S. Letizia and A. M. Api, Fragrance material review on methyl salicylate, *Food Chem. Toxicol.*, 2007, **45**, 428–452.

66 J. Lewiński, J. Zachara, B. Mańk and S. Pasynkiewicz, Synthesis and Molecular Structure of AlMe[O·C(OMe)C_6H_4-o-O]$_2$. The First Structurally Characterized Five-Coordinated Simple Alky, *J. Organomet. Chem.*, 1993, **454**(1–2), 5–7.

67 J. Lewiński, J. Zachara and K. B. Starowieyski, Structure Investigation of Dimethyl-Aluminium, -Gallium and -Indium O,O′-Chelate Complexes in Solution and the Solid State. Molecular Structure of Five-Co-Ordinated $[Me_2M(\mu\text{-}OC_6H_4CO_2Me\text{-}2)]_2$ Adducts, *J. Chem. Soc., Dalton Trans.*, 1997, **22**, 4217–4222.

68 R. N. Duffin, V. L. Blair, L. Kedzierski and P. C. Andrews, Alkyl gallium(III) quinolinolates: A new class of highly selective anti-leishmanial agents, *Eur. J. Med. Chem.*, 2020, **186**, 111895.

69 L. G. Bloor, C. J. Carmalt and D. Pugh, Single-source precursors to gallium and indium oxide thin films, *Coord. Chem. Rev.*, 2011, **255**, 1293–1318.

70 C. J. Carmalt and S. J. King, Gallium(III) and indium(III) alkoxides and aryloxides, *Coord. Chem. Rev.*, 2006, **250**, 682–709.

71 T. Li, R. Fang, B. Wang, Y. Shao, J. Liu, S. Zhang and Z. Yang, A Simple Coumarin as a Turn-on Fluorescence Sensor for Al(III) Ions, *Dalton Trans.*, 2014, **43**(7), 2741–2743.

72 S. Müller, S. Steil, A. Droghetti, N. Großmann, V. Meded, A. Magri, B. Schäfer, O. Fuhr, S. Sanvito, M. Ruben, M. Cinchetti and M. Aeschlimann, Spin-Dependent Electronic Structure of the Co/Al$(OP)_3$ Interface, *New J. Phys.*, 2013, **15**(11), 113054.

73 A. R. Sanwaria, M. Nagar, R. Bohra, A. Chaudhary, S. M. Mobin, P. Mathur and B. L. Choudhary, Sol–Gel Synthesis of Highly Pure α-Al2O3 Nano-Rods from a New Class of Precursors of Salicylaldehyde-Modified Aluminum(Iii) Isopropoxide. Crystal and Molecular Structure of $[Al(OC_6H_4CHO)_3]$, *RSC Adv.*, 2014, **4**(57), 30081–30089.

74 H. C. Aspinall, J. Bacsa, O. D. Beckingham, E. G. B. Eden, N. Greeves, M. D. Hobbs, F. Potjewyd, M. Schmidtmann and C. D. Thomas, Adding the Right (or Left) Twist to Tris-Chelate Complexes–Coordination Chemistry of Chiral Oxazolylphenolates with M^{3+} Ions (M = Al or Lanthanide), *Dalton Trans.*, 2014, **43**(3), 1434–1442.

75 M. A. Bahili, E. C. Stokes, R. C. Amesbury, D. M. C. Ould, B. Christo, R. J. Horne, B. M. Kariuki, J. A. Stewart, R. L. Taylor, P. A. Williams, M. D. Jones, K. D. M. Harris and B. D. Ward, Aluminium-Catalysed Isocyanate Trimerization, Enhanced by Exploiting a Dynamic Coordination Sphere, *Chem. Commun.*, 2019, **55**(53), 7679–7682.

76 J. E. Bollinger, J. T. Mague and D. M. Roundhill, Lipophilic Hexadentate Aluminum, Gallium, Indium, and Iron Complexes of a New Phenolate-Derivatized Cyclohexanetriamine Ligand, *Inorg. Chem.*, 1994, **33**(7), 1241–1242.

77 S. Alvarez, Distortion Pathways of Transition Metal Coordination Polyhedra Induced by Chelating Topology, *Chem. Rev.*, 2015, **115**, 13447–13483.

78 H. Schumann, M. Frick, B. Heymer and F. Girgsdies, Intramolecularly Stabilized Organoaluminium and Organogallium Compounds: Synthesis and X-Ray Crystal Structures of Some Dimethylaluminium and -Gallium Alkoxides Me_2M–O–R–OR′ and Amides Me_2M–NH–R–OR′, *J. Organomet. Chem.*, 1996, **512**(1–2), 117–126.

79 C. E. Knapp, L. Pemberton, C. J. Carmalt, D. Pugh, P. F. McMillan, S. A. Barnett and D. A. Tocher, Synthesis, AACVD and X-Ray Crystallographic Structures of Group 13 Monoalkoxometallanes, *Main Group Chem.*, 2010, **9**(1,2), 31–40.

80 P. Horeglad, M. Cybularczyk, A. Litwińska, A. M. Dąbrowska, M. Dranka, G. Z. Żukowska, M. Urbańczyk and M. Michalak, Controlling the Stereoselectivity of Rac-LA Polymerization by Chiral Recognition Induced the Formation of Homochiral Dimeric Metal Alkoxides, *Polym. Chem.*, 2016, **7**(11), 2022–2036.

81 D. G. Hendershot, M. Barber, R. Kumar and J. P. Oliver, Synthesis and Characterization of Alkylaluminum and -Gallium Derivatives of 2-(Methylthio)- and 2-Methoxyphenol. Crystal Structures of the Dimeric Complexes $[R_2M(\mu\text{-}OC_6H_4\text{-}2\text{-}ECH_3)]_2$ (M = Aluminum, E = S, R = Me, Iso-Bu; M = Al, E = O, R = Et, Iso-Bu; M = Gallium, E = O, R = Me) Featuring Five Coordinate Metal Centers, *Organometallics*, 1991, **10**(9), 3302–3309.

82 C. E. Knapp and C. J. Carmalt, Solution Based CVD of Main Group Materials, *Chem. Soc. Rev.*, 2016, **45**(4), 1036–1064.

83 L. G. Bloor, C. J. Carmalt and D. Pugh, Single-Source Precursors to Gallium and Indium Oxide Thin Films, *Coord. Chem. Rev.*, 2011, **255**(11–12), 1293–1318.
84 W. Ziemkowska, Group 13 Alkyl Compounds Incorporating Aliphatic and Aromatic Diolate Ligands, *Coord. Chem. Rev.*, 2005, **249**(21–22), 2176–2194.
85 J. A. Francis, S. G. Bott and A. R. Barron, Are intramolecularly stabilized compounds of aluminum suitable structural models of the SN_2 transition state? Molecular structure of $[(^tBu)_2Al(\mu\text{-}OC_6H_4\text{-}2\text{-}OMe)]_2$, *Polyhedron*, 1999, **18**, 2211–2218.
86 C. N. McMahon, S. G. Bott and A. R. Barron, Observation of an unusual amine oxidation reaction during the oxidation and hydrolysis of $[(^tBu)_2Ga(o,\text{-}C_6H_4NMe_2)]_2$: molecular structures of $(^tBu)_2Ga(o\text{-}C_6H_4NMe_2)(\mu\text{-}OH)\text{-}Ga(^tBu)[o\text{-}C_6H_4N(O)Me_2]$ $(^tBu)_2Ga(o\text{-}C_6H_4NMe_2)(O{=}PPh_3)$, *Polyhedron*, 1997, **16**, 3407–3413.
87 W. Clegg, E. Lamb, S. T. Liddle, R. Snaith and A. E. H. Wheatley, Towards an Understanding of the Conjugate Addition of Organolithium Reagents to α,β-Unsaturated Ketones: The Isolation and Solid-State Structure of a Monomeric Lithium Aluminate with Very Short Agostic Li···HC Interactions, *J. Organomet. Chem.*, 1999, **573**(1–2), 305–312.
88 M. B. Power, A. R. Barron, S. G. Bott and J. L. Atwood, . Pi.-Face Selectivity of Coordinated Ketones to Nucleophilic Additions: The Importance of Aluminum-Oxygen .Pi.-Bonding, *J. Am. Chem. Soc.*, 1990, **112**(9), 3446–3451.
89 X. Pan, A. Liu, L. Yao, L. Wang, J. Zhang, J. Wu, X. Zhao and C.-C. Lin, Synthesis, Characterization of Hetero-Bimetallic Complex and Application in the Polymerization of ε-Caprolactone, *Inorg. Chem. Commun.*, 2011, **14**(5), 763–766.
90 H. Nöth, A. Schlegel and M. Suter, A Study of Noyori's Reagent, *J. Organomet. Chem.*, 2001, **621**(1–2), 231–241.
91 M. T. Muñoz, C. Urbaneja, M. Temprado, M. E. G. Mosquera and T. Cuenca, Lewis Acid Fragmentation of a Lithium Aryloxide Cage: Generation of New Heterometallic Aluminium-Lithium Species, *Chem. Commun.*, 2011, **47**(42), 11757–11759.
92 H. Bock, R. Beck, Z. Havlas and H. Schödel, Tetralithium Bis(Ethylaluminum) Tetrakis(Catecholate) Pentakis (Dimethoxyethane): An Oxygen-Rich Cluster $[(Al^{++}{}_2(Li^+)_4(O18)^{-8}]$ in a $C_{36}H_{44}$ Hydrocarbon Shell, *Eur. J. Inorg. Chem.*, 1998, **1998**(12), 2075–2077.
93 H. Bock, R. Beck, Z. Havlas and H. Schodel, Preparation, Structure, and Density Functional Calculation of the Solvent-Separated Ion Pair $[(H_5C_2)Al(OC_6H_5)_3{}^-\cdots Li^+\cdots{}^-(H_5C_6O)_3Al(C_4H_9)]^-[Li^+(DME)_3]$, *Inorg. Chem.*, 1998, **37**, 5046–5049.
94 S. M. Ivanova, B. G. Nolan, Y. Kobayashi, S. M. Miller, O. P. Anderson and S. H. Strauss, Relative Lewis Basicities of Six $Al(OR_F)^{4-}$ Superweak Anions and the Structures of $LiAl\{OCH(CF_3)_2\}_4$ and $[1\text{-Et-}3\text{-Me-}1,3\text{-}C_3H_3N_2][Li\{Al\{OCH(CF_3)_2\}_4\}_2]$, *Chem. – Eur. J.*, 2001, **7**(2), 503–510.
95 S. Alvarez, P. Alemany, D. Casanova, J. Cirera, M. Llunell and D. Avnir, Shape maps and polyhedral interconversion paths in transition metal chemistry, *Coord. Chem. Rev.*, 2005, **249**, 1693–1708.
96 A. J. Blake, A. Cunningham, A. Ford, S. J. Teat and S. Woodward, Enantioselective Reduction of Prochiral Ketones by Catecholborane Catalysed by Chiral Group 13 Complexes, *Chem. – Eur. J.*, 2000, **6**(19), 3586–3594.
97 P. C. Andrews, C. M. Forsyth, P. C. Junk, I. Nuzhnaya and L. Spiccia, Synthesis and Structural Characterisation of Gallium and Indium Fluoroalkoxide 'Ate' Complexes, *J. Organomet. Chem.*, 2009, **694**(3), 373–381.
98 J. Pauls, S. Chitsaz and B. Neumüller, Chiral Gallium and Indium Alkoxometalates, *Z. Anorg. Allg. Chem.*, 2000, **626**(9), 2028–2034.
99 E. Jung, S. H. Yoo, T.-M. Chung, C. G. Kim, Y. Kim and D. Y. Jung, Heterobimetallic Lithium Organoaluminum and Organogallium Complexes: Potential Single Precursors for MOCVD of $LiMO_2$ Thin Films, *Inorg. Chem. Commun.*, 2002, **5**(6), 439–441.
100 I. Arvanitoyannis, A. Nakayama, N. Kawasaki and N. Yamamoto, Novel Star-Shaped Polylactide with Glycerol Using Stannous Octoate or Tetraphenyl Tin as Catalyst: 1. Synthesis, Characterization and Study of Their Biodegradability, *Polymer*, 1995, **36**(15), 2947–2956.
101 M. Bednarek, Branched Aliphatic Polyesters by Ring-Opening (Co)Polymerization, *Prog. Polym. Sci.*, 2016, **58**, 27–58.
102 Y. Zhu, C. Romain, V. Poirier and C. K. Williams, Influences of a Dizinc Catalyst and Bifunctional Chain Transfer Agents on the Polymer Architecture in the Ring-Opening Polymerization of ε-Caprolactone, *Macromolecules*, 2015, **48**, 2407–2416.
103 A. B. Kremer, R. J. Andrews, M. J. Milner, X. R. Zhang, T. Ebrahimi, B. O. Patrick, P. L. Diaconescu and P. Mehrkhodavandi, A Comparison of Gallium and Indium Alkoxide Complexes as Catalysts for Ring-Opening Polymerization of Lactide, *Inorg. Chem.*, 2017, **56**(3), 1375–1385.
104 S.-C. Rosca, D.-A. Rosca, V. Dorcet, C. M. Kozak, F. M. Kerton, J.-F. Carpentier and Y. Sarazin, Alkali aminoether-phenolate complexes: synthesis, structural characterization and evidence for an activated monomer ROP mechanism, *Dalton Trans.*, 2013, **42**, 9361–9375.
105 Agilent, *CrysAlis PRO*, Agilent Technologies Ltd, Yarnton, Oxfordshire, England, 2014.
106 G. M. Sheldrick, Crystal Structure Refinement with SHELXL, *Acta Crystallogr., Sect. C: Struct. Chem.*, 2015, **71**, 3–8.
107 K. Brandenburg, *DIAMOND*, Crystal Impact GbR, Bonn, Germany, 2007.
108 R. Petrus, P. Fałat and P. Sobota, Use of Lithium Aryloxides as Promoters for Preparation of α-Hydroxy Acid Esters, *Dalton Trans.*, 2020, **49**(3), 866–876.

